RSC Advances

REVIEW

View Article Online
View Journal | View Issue

Cite this: *RSC Adv.*, 2023, **13**, 17883

Nano-biosensor for SARS-CoV-2/COVID-19 detection: methods, mechanism and interface design

Yansheng Liu,*[ab] Zhenle Qin,[a] Jin Zhou,[a] Xiaobo Jia,[a] Hongli Li,[a] Xiaohong Wang,[a] Yating Chen,[a] Zijun Sun,[a] Xiong He,[a] Hongda Li,[ab] Guofu Wang*[a] and Haixin Chang*[b]

The epidemic of coronavirus disease 2019 (COVID-19) was a huge disaster to human society. The severe acute respiratory syndrome coronavirus 2 (SARS-CoV-2), which led to COVID-19, has resulted in a large number of deaths. Even though the reverse transcription-polymerase chain reaction (RT-PCR) is the most efficient method for the detection of SARS-CoV-2, the disadvantages (such as long detection time, professional operators, expensive instruments, and laboratory equipment) limit its application. In this review, the different kinds of nano-biosensors based on surface-enhanced Raman scattering (SERS), surface plasmon resonance (SPR), field-effect transistor (FET), fluorescence methods, and electrochemical methods are summarized, starting with a concise description of their sensing mechanism. The different bioprobes (such as ACE2, S protein-antibody, IgG antibody, IgM antibody, and SARS-CoV-2 DNA probes) with different bio-principles are introduced. The key structural components of the biosensors are briefly introduced to give readers an understanding of the principles behind the testing methods. In particular, SARS-CoV-2-related RNA mutation detection and its challenges are also briefly described. We hope that this review will encourage readers with different research backgrounds to design SARS-CoV-2 nano-biosensors with high selectivity and sensitivity.

Received 18th April 2023
Accepted 26th May 2023

DOI: 10.1039/d3ra02560h

rsc.li/rsc-advances

1. Introduction

In December of 2019, the first unknown outbreak of a new type of pneumonia was discovered in the city of Wuhan, Hubei Province, in China. Further, numerous infected cases were

[a]*School of Electronic Engineering, Guangxi University of Science and Technology, Liuzhou 545616, Guangxi, China*

[b]*Quantum-Nano Matter and Device Lab, State Key Laboratory of Material Processing and Die and Mould Technology, School of Materials Science and Engineering, Huazhong University of Science and Technology Wuhan, 430074, Hubei, China*

Liu Yansheng is an Associate Researcher at the Guangxi University of Technology. He was awarded an honorary doctorate title by Universidad Autónoma de Madrid in 2020 in Spain. He completed his research at the Madrid Institute for Advanced Studies of Materials (IMDEA) under the supervision of Prof. Dr Feng Luo and Prof. Dr Rodolfo Miranda Soriano. His research interests are surface-enhanced Raman scattering, and its application in the detection of molecules under extremely low concentrations and biomaterials such as DNA and virus. Nowadays, he is working on detecting Covid-19 in human secretions.

Guofu Wang is a Professor at the Guangxi University of Technology. He received his M.S. and PhD degrees in signal and information processing from the Chinese Academy of Sciences, in 2005 and 2007, respectively. He worked at Guilin University of Electronic Technology before moving to the Guangxi University of Technology in 2017. He has been a Professor with the School of Electrical and Information Engineering, Guangxi University of Technology. His main research interest is next-generation information technology.

diagnosed, and deaths were gradually reported. On January 20, 2020, the city of Wuhan was blocked to avoid the spread of this pneumonia-like illness that was later named COVID-19 disease. In the following months, the SARS-CoV-2 virus that caused the COVID-19 epidemic spread quicky throughout the world. In the following year, the SARS-CoV-2 vaccine[1] was developed against the virus. Even though a lot of effort has been made by countries around the world to control and fight against the SARS-CoV-2 virus, it still is spreading and affecting both people who have been inoculated with vaccines or have not been inoculated. SARS-CoV-2 possesses the characteristics of strong transmission ability, strong infection ability, strong mutation ability, long incubation period, and long survival time.[2] These properties make the global anti-epidemic work with great difficulty. It has been widely accepted that the main means of SARS-CoV-2 spreading are touching, viral aerosol, air contamination, the oral-fecal route, blood, from mothers to newborns, and animals to humans.[3,4] Thus far, mutated viruses such as Omicron, Delta, and Alpha SARS-CoV-2 variants are widely observed and recognized.[5]

A coronavirus (CoVs) is an enveloped virus that entraps non-segmented ribonucleic acid (ssRNA), positive sense, and single strand. The CoVs have a genome size of 26 to 32 kb, which is the largest RNA virus known today.[6] SARS-CoV-2 is a member of the coronaviruses family and it belongs to β-coronaviruses.[7,8] SARS-CoV-2 possesses a crown-shaped appearance with a diameter of 60–140 nm, which has been observed using transmission electron microscopy.[9] The complete genome of SARS-CoV-2 was reported by Khailany *et al.*[10] Fig. 1 illustrates the SARS-CoV-2 structure,[8,11,12] which consists of a spike protein (S), an envelope protein (E), membrane protein (M), and nucleocapsid (N) proteins. The M and E proteins form the virus envelope, and the N protein responds by assembling the virus.[13] The S protein is the key protein for viruses to invade susceptible cells, and it plays a crucial role in infection.[14] The S protein is a homotrimer,[15] and each monomer is folded and glycosylated by sialic acid distally.[16] The host proteases cleave the S protein into two subunits, S1 and S2. The S2 subunit acts as an anchor to bind the viral membrane and it responds to the virus fusion with the host cell.[15] The S1 subunit plays a role in cell recognition, cell invasion, and antibody neutralization.[17] The invasion process of SARS-CoV-2 is mediated by the binding between the S1 subunit and angiotensin-converting enzyme 2 (ACE2), which acts as a receptor on the host cell cytomembrane.[18–22]

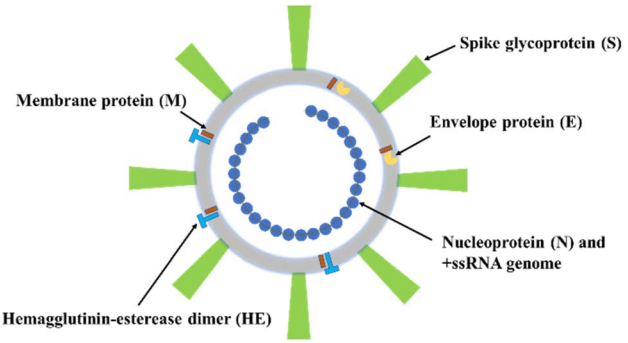

Fig. 1 Scheme of the SARS-CoV-2 structure. SARS-CoV-2 is an enveloped, positive-sense RNA virus with four main structural proteins that are spike (S) and membrane (M) glycoproteins, as well as envelope (E) and nucleocapsid (N) proteins.

At present, two detection categories for detecting SARS-CoV-2 are widely applied, which are gold immunochromatography assay (GICA) and viral polymerase chain reaction (PCR).[23–27] The humoral immune response generates SARS-CoV-2 antibodies approximately 1 week or more after infection.[28] In older adults, children, and patients with immune deficiency disease, the antibody production capacity is lower in immune-compromised humans, which may lead to a potentially false categorization or delayed diagnosis.[29] In the GICA, SARS-CoV-2 can be detected by detecting IgG or IgM antibodies. Since IgM antibodies in the blood can be detected after the infection of 3–6 days, and IgG antibodies can only be detected 8 days after infection, the antibody detection misses the window period of prevention of the SARS-CoV-2 epidemic. PCR can recognize virus-infected cases at an early stage with high confidence and detection limits of a few copies. PCR requires a high level of amplification of the oligonucleotide, in which the nucleic acid contaminants introduced in the sampling process or amplification steps may also serve as templates, resulting in inaccurate assay results.[30] Moreover, the inhibitor used in the propagation of viral nucleic acid is a threat to the enzymatic amplification reaction. Usually, the product after propagation needs to be further purified, which makes the PCR complicated and cumbersome.[31] Studies have shown that the reporting rate of the PCR "false negative" results is as high as 20% to 40% when re-examining suspected cases through medical images.[23] This result indicates that the reliability of PCR, which is regarded as a "gold standard" in detecting SARS-CoV-2 in practice, is decreased due to its relatively complicated operation process. Therefore, it is of great significance to develop and research key technologies for the

Haixin Chang is a Full Professor at Huazhong University of Science and Technology. He obtained his PhD in Materials Science in 2007 from the Institute of Metal Research, Chinese Academy of Sciences. Then, he worked in the Department of Chemistry, Tsinghua University, and Nanotechnology Centre, ITC, Hong Kong Polytechnic University, before moving to Tohoku University at the beginning of 2011. He joined the faculty of Tohoku University as an assistant professor in 2012. He joined the Huazhong University of Science and Technology as a Full Professor in 2014. His research studies focus on graphene, 2D/quantum materials and physics, 2D electronics/optoelectronics, and new energy materials. He has published over 80 papers with a citation over 5500 times. He was also awarded in 2020 and 2021 as an Elsevier Highly Cited Chinese Researcher.

rapid, efficient, highly sensitive, and economical virus detection of SARS-CoV-2.

The basic principle of nano-biosensors is to convert the biometric information to optical or electrical signals, which can be directly observed. Its fast, sensitive, reliable, and easy-to-use characteristics are suitable for the detection of SARS-CoV-2. By combining the specific bio-probe (*e.g.*, S protein, ACE2, antibody, and viral RNA sequence) with a sensitive physical and chemical sensor, the target biomolecules could be specifically detected. Until now, different kinds of nano-biosensors have been designed and fabricated in detecting bio-materials, such as proteins, oligonucleotides, and viruses. In this review, the nano-biosensors based on optical and electrical methods are collected and presented. The physical/chemical mechanisms are presented, as well as the brief fabrication process. A comparable discussion of each kind of biosensor is presented. The section discusses the possibility of detecting mutated SARS-CoV-2 has been individually given.

2. Bio-probes for detecting SARS-CoV-2

The S protein is the most exposed viral protein on the SARS-CoV-2 virion surface. In the invasion process of SARS-CoV-2, the S protein is responsible for receptor recognition and membrane fusion.[32] S1 subunits of the S protein have the receptor binding domain (RBD) that can interact directly with the ACE2 peptidase domain (PD).[33] Meanwhile, the subunits S2 of the S protein play a role in membrane fusion. The cooperation of S1 and S2 with the assistance of ACE2 make the SARS-CoV-2 affect humans. So, ACE2 can be applied as a bio-probe in detecting SARS-CoV-2 through the ACE2-S protein pair. Except for the S protein, N protein detection as an outer structure of the SARS-CoV-2 virus also has been applied as an RBD, and the N protein antibody is the bio-probe. For each virus, the genome sequence is unique. The size of the genome sequence length of SARS-CoV-2 is around 30 kb, with a 5′-cap structure and 3′-poly-(A) tail enveloped by a complex of structural proteins.[34] Due to this uniqueness of the genome sequence, the perfectly matched nucleic acid sequence is manually fabricated to selectively bind to the target RNA sequence of the SARS-CoV-2. IgG and IgM are processed by the human body when the SARS-CoV-2 invades healthy cells. IgG and IgM can specifically bind to the SARS-CoV-2 coronavirus antigen. So, IgG/IgM antibodies are good bioprobes in the detection of SARS-CoV-2.

3. Surface-enhanced Raman scattering (SERS)

Raman spectroscopy is a very important, promising, and powerful technique in characterizing the structure of chemical materials or bio-material without any damage. The discovery of wavelength-shifted scattering occurred from 1922 to 1923.[35] In 1928, C. V. Raman found "a new radiation", which is now widely known as the Raman effect.[36,37] In the process of Raman scattering, incident light excites the molecules, and most of the photons are scattered in an elastic way with energy maintained. The minority of photons are scattered inelastically with energy loss or gain. Raman scattering can provide vibrational information about molecules, but only 10^6 to 10^8 photons illuminated on the sample can undergo Raman scattering. The remaining photons experience competing pathways, such as fluorescence, Rayleigh elastic scattering, and heating.[38] Surface-enhanced Raman scattering (SERS) as a surface sensing technique has been widely applied in the ultrasensitive and selective detection in biology and chemistry.[39–41] By applying the proper SERS-enhanced substrate, the Raman signals could be largely enhanced.[42] Until now, SERS is the only capable method for simultaneously detecting a single molecule and providing its chemical fingerprint.[43–47] For SERS, two mechanisms are widely accepted, which are the chemical mechanism (CM) and the electromagnetic mechanism (EM).[48,49] CM is formed by a charge transfer between the target molecule and the substrate. It usually has a minor enhancement factor of 10 to 100.[44] CM is commonly referred to as the "first layer effect" because of the small distances needed for charge transfer. In some studies, the first monolayer molecules absorbed on the substrate often show a much larger SERS cross-section than the second layer.[50] Such a reason necessitated a small uniform rough surface to obtain an improved chemical signal. The localized electromagnetic field caused by surface excitation plasmon (SPs) is the basis of the EM mechanism. SP is the coherent oscillation of conduction electrons under the condition of light illumination.[51–53] The light-induced electromagnetic field results in a significant increment of the cross-section of the Raman scattering, and the Raman enhancement factor could reach up to 10^8 or more.[50,54,55] To achieve higher SERS performance, easily fabricated metallic nanostructures are the most common and useful SERS-enhanced materials. The most used materials are Au and Ag, which can induce larger electromagnetic fields under light excitation. It has been proved that the higher SERS performance occurs at the edge of the metallic structures.[48,56] Different kinds of metallic nanomaterials with verifying morphology have been designed and applied in SERS, which illustrate good performance such as nanodisks,[57,58] nanopores,[59–61] nanopillar,[62,63] nanoparticles,[64,65] nanoprime,[66,67] nano spheres,[68] nanostar,[69] nanocubic,[70] nanooctahedron[71] and nanowires.[72] Wang[73] designed and fabricated an Au@Ag core–shell structure with a strong localized plasma resonance effect. By applying the 4-MBA (4-mercaptobenzoic acid) as reporter molecules, he could detect the prostate-specific antigen with a LOD of 0.94 fg mL^{-1}. Ganesh[74] designed a quantum organic semiconductor with a strong charge-transfer effect with bio-molecules, and applied it to detect DNA in the cancer cell. Due to the CM mechanism of SERS, the SERS signal was enormously enhanced and the LOD was 10^{-15} mol L^{-1}. By analyzing the SERS spectra, Ganesh decoded the bases of the cancer genome, and revealed the expression of genomic DNA variation.[74] Huang[75] used disordered gold nanopores as SERS substrates, and successfully analyzed the order of bases in oligonucleotides through the SERS spectra. Owing to the high sensitivity and selectivity, SERS illustrates the great potential in the detection of SARS-CoV-2.

Except for the morphology-dependent SERS performance, the gap between the coherent nanostructures also affects the enhanced SERS intensity. It has been widely accepted that the smaller gap results in larger SERS enhancement factors.[80–82] Ojodomo J. Achadu[76] reported that a 3-dimensional porous magnetic nanoparticle 3D mag-MoO_3–PDA@Au NS (molybdenum trioxide–polydopamine-gold functionalized nanosphere) was designed as SERS "hot spots" in detecting SARS-CoV-2 (Fig. 2a). By applying an external magnetic field, the aggregated 3D mag-MoO_3–PDA@Au NS showed an unprecedented SERS amplification. ACE2 was used as a bio-probe to specifically bind to the SARS-CoV-2 spike protein, which was applied as an analyte. During his experiments, the smaller nanogap between the coherent magnetic nanoparticles was magnetically induced by an external magnetic field, which resulted in high SERS performance. Meanwhile, the smaller gaps can generate the sandwich architecture that is the (NS-ACE2)-(S protein)-(ACE2-NS) structure. In this sandwich architecture, the SERS signal binding between the ACE2-(S protein) was largely enhanced with a detection limit of 4.5 fg mL^{-1}.

SERS can directly identify the structural information of analytes. Yusi Peng[77] used Nb_2C and Ta_2C MXenes as SERS substrates to directly identify the SARS-CoV-2 S protein with a LOD of 5×10^{-9} mol L^{-1} (Fig. 2b). However, direct identification methods are mainly applied in detecting pre-purified molecules. For complex compounds, the overlap of the characterized SERS peaks limits its application in detecting SARS-CoV-2 due to multi-component samples. The application of a bio-probe is more reliable in detecting SARS-CoV-2. ACE2 and the S protein antibody are important molecules that can bind to the S protein of SARS-CoV-2. The ACE2 possesses strong characteristic Raman peaks, and the intensities of some characteristic peaks are reduced when the interaction occurs between ACE2 and S protein[78] (Fig. 2c). By analyzing the intensity change of the characteristic peaks (*e.g.*, 1189 cm^{-1}) of ACE2 and the appearance of a signal at 1182 cm^{-1} belonging to the SARS-CoV-2 virus, it was easy to confirm the existence of the SARS-CoV-2 virus. The SERS performance of biomolecules is relatively weak. To enhance the SERS intensities,[83] the Raman-sensitive molecules are always selected as indicators, which were used to label the bioprobes. Zhang[79] used 4-MBA (4-mercaptobenzoic acid)-labeled Ag NPs as SARS-CoV-2 spike antibody nano-tags (Fig. 2d). The few-layer Au NPs modified by the SARS-CoV-2 spike antibody were fabricated as SERS-immune substrates. This SERS-based sandwich biosensor can detect the SARS-CoV-2 spike protein with a LOD of 0.77 fg mL^{-1} in phosphate-buffered saline and 6.07 fg mL^{-1} in untreated saliva, respectively. In addition, this biosensor is able to detect the SARS-CoV-2 spike protein in serum and blood with the LOD of 7.60 fg mL^{-1} and 0.10 pg mL^{-1}, respectively.

The testing of IgG and IgM antibodies is a good method for COVID-19 diagnosis. It has been reported that the anti-SARS-CoV-2 IgM/IgG antibodies are detectable within 0–5 days after symptom onset.[86] Normally, lateral flow immunoassay (LFIA) methods are widely applied to detect anti-SARS-CoV-2 IgM/IgG antibodies. In a typical LFIA process, a liquid sample containing the target analytes flows along the strip.[87] During the movement of the sample, the target analytes are labeled by

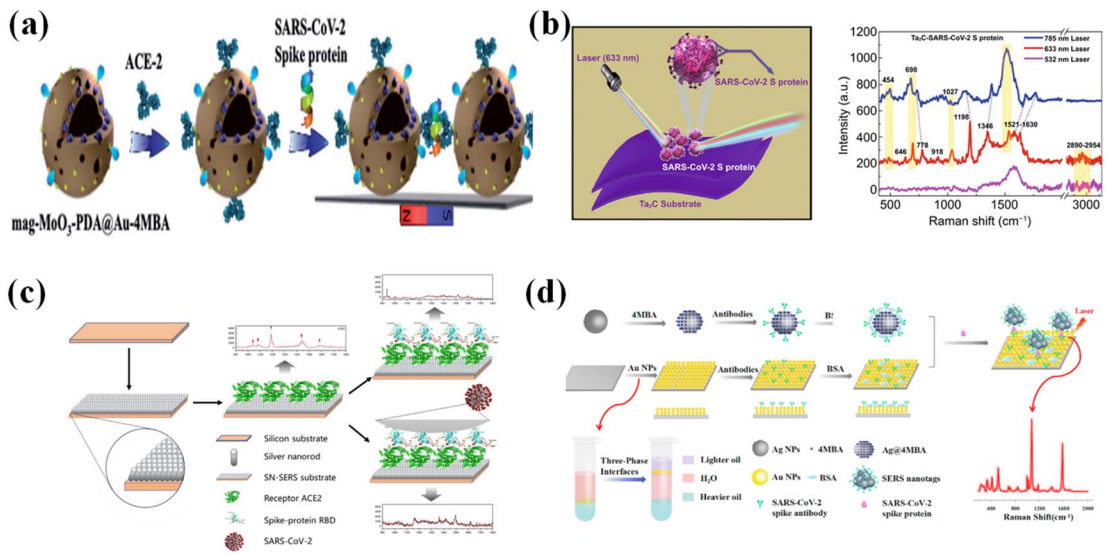

Fig. 2 (a) Diagram of the 3D mag-MoO_3-PDA@Au nanostructure modified with ACE2 acting as SERS material, and scheme of the sandwich structure after immunoreaction with a spike protein. Reprinted with permission from ref. 76. (b) Raman schematic diagram and the SERS spectra of the Ta_2C nano-sheets (NSs) for the Raman scattering of the SARS-CoV-2 S protein with a concentration of 10^{-9} mol L^{-1} under the excitation laser at 532, 633, and 785 nm. Reproduced with permission from ref. 77. (c) State-of-the-art diagram of silver-nanorod SERS (SN-SERS) substrate functionalized with ACE2 for interrogating SARS-CoV-2. The ACE2@SN-SERS array generated strong SERS signals that were significantly quenched after the binding of the SARS-CoV-2 spike protein. Adapted with permission from ref. 78. (d) Schematic illustration of the SERS-based immunoassay. The 4-MBA labeled AgNPs-antibody and AuNPs-antibody layers were both stabilized by BSA, and they were applied to form a (4MBA-AgNPs-antibody)-(S protein)-(AuNPs-antibody) sandwich structure that illustrates good detecting sensitivity. Adapted with permission from ref. 79.

metallic Au NPs and then flow to the test lines. The test lines are functionalized with probes that can specifically bind to the analyte and illustrate a color change.[88,89] However, LFIA is based on colorimetric analysis, and it has the disadvantage of low sensitivity and poor quality. The SERS-LFIA method is a good candidate for diagnosing COVID-19 through strong, specific, and stable SERS signals.[90–94] In a study by Haifeng Liu,[84] the SARS-CoV-2 IgM/IgG antibodies in clinical samples were analyzed through a SERS-LFIA in 25 minutes (Fig. 3a–c). Shiliang Chen[85] also performed similar work in which the IgM and IgG test lines were integrated on the same strip (Fig. 3d and e). The LOD for IgM and IgG were 1 and 0.1 ng mL^{-1}, respectively.

These methods, combined with artificial intelligence (AI), are a promising way to distinguish small changes in the optic spectra, and it is meaningful in SARS-CoV-2 detection. In principle, SERS can be directly applied in detecting SARS-CoV-2 without any probes or labels. However, unexpected organic compounds always coexist when taking samples from human bodies. The mixed sample shows a complex SERS spectrum, which makes it very difficult to distinguish the characteristic peaks of SARS-CoV-2. In such a case, deep learning could help.[96] Deep learning methods combined with SERS have been widely applied in analyzing bio or chemical materials, such as cancers,[97,98] bacterial lysate,[99] honey varieties,[100] and viruses.[101] In the study of Jinglin Huang,[95] the Ag NPs-coated Si was applied as a SERS substrate to detect the SARS-CoV-2 antigen (Fig. 4). In his study, a deep learning model was applied to train to distinguish the SERS detection spectrum of S proteins of SARS-CoV-2, SARS-CoV, and Middle East respiratory syndrome coronavirus (MERS-CoV), and the model illustrated an identification accuracyof 87.7%. C. Carlomagno[102] also designed

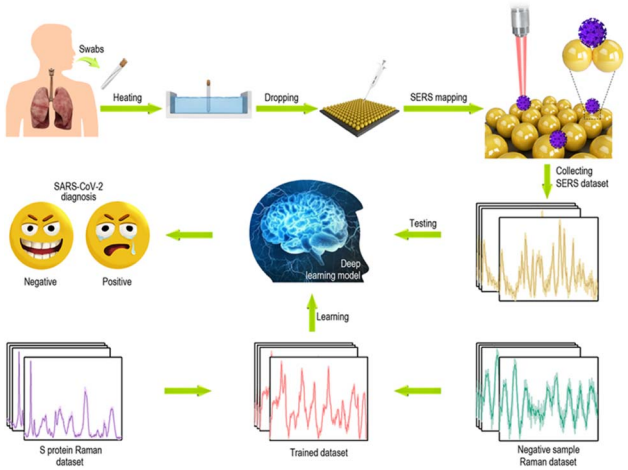

Fig. 4 Schematic illustration of the detection process of the deep learning-based SERS technique. Adapted with permission from ref. 95.

a deep learning model for detecting SARS-CoV-2 in saliva samples with an accuracy within the range of 89% to 92%. These methods, combined with artificial intelligence (AI), is a promising way to distinguish small changes of the optic spectra, and it is meaningful in SARS-CoV-2 detection.

Breath volatile organic compounds (BVOCs) analysis is a non-invasive method that allows for analyzing cancer at an early stage through analyzing biomarkers in exhaled breath.[104] Interesting research has been performed by Shi Xuan Leong,[103] who came up with a strategy for directly identifying infection of SARS-CoV-2 by combining SERS with breath volatile organic compounds (BVOCs) (Fig. 5). SARS-CoV-2 is a virus that can

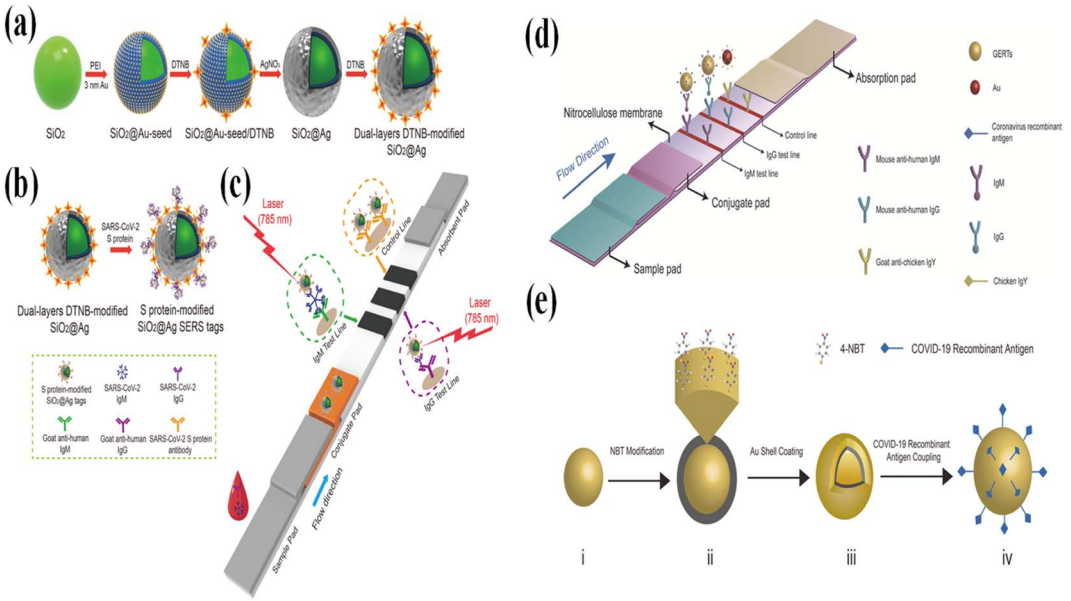

Fig. 3 (a) Scheme of the preparation of the dual-layers DTNB-modified SiO_2@Ag NPs, in which the DTBA acts as indicators. (b) Image of the preparation of the SARS-CoV-2 S protein-modified SiO_2@Ag SERS tags. (c) Operating principle of the high-sensitivity and simultaneous analysis of anti-SARS-CoV-2 IgM/IgG *via* the SERS-LFIA strip. Adapted with permission from ref. 84. (d) Schematic diagram of the SERS-based strip for the detection of IgM and IgG. (e) Scheme of the preparation for the Au core@4-NBT@Au shell structure. Reproduced with permission from ref. 85.

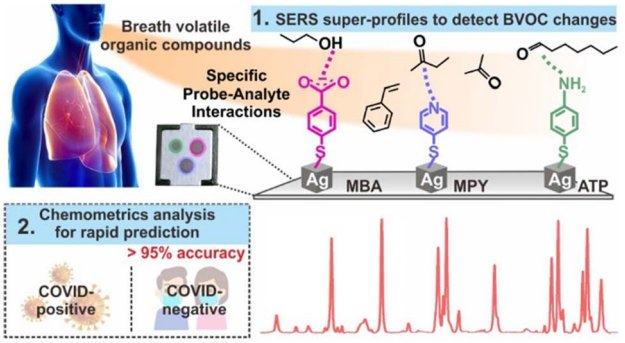

Fig. 5 The mechanism of detecting breath volatile organic compounds (BVOCs) changes by using SERS with an accuracy of 95%. Adapted with permission from ref. 103.

cause pneumonia, which makes the BVOCs a method of detecting SARS-CoV-2 with an innate advantage. It has been reported that the coronavirus can induce immune responses and metabolic changes, which has been confirmed by analyzing the changing of aldehydes, ketones, and alcohols in exhaled breath.[105,106] Normally, mass spectra are widely applied in detecting BVOCs[107,108] with a sensitivity and specificity of around 80%. However, it is a time-consuming and money-consuming method. The combination of Raman spectra and BVOCs technique illustrates advantages, such as being simple, portable, and inexpensive.

SERS sensors combine the detection of optical physical information and biological chemical information, and can achieve ultrahigh sensitivity with high selectivity. However, to achieve the best performance, the morphology of the SERS substrate formed by the noble metal needs to be optimized for best Raman signal enhancement. In addition, the repeatable utilization of the SERS sensor and the specially designed noble metal substrate are challenging for developing low-cost SARS-CoV-2 sensors. Finally, SERS needs a relatively complicated Raman system to support the collection of high-resolution Raman spectra for high-sensitivity detection. The commercially-available fiber-based Raman system has been limited by low resolution in Raman spectra. Therefore, the development of compact, high-resolution, convenient, reusable SERS systems and sensors is highly desirable.

4. Surface plasmon resonance (SPR)

Surface plasmon resonance (SPR) is a collection of oscillations of free electrons on a metal surface that is induced by incident light. The first application of the SPR biosensor was designed by Liebenberg and Nylander in 1982.[109] Since then, the SPR biosensor as a surfacing sensing technique has been widely applied in the interdisciplinary study between chemistry, physics, and biology.[110] Nowadays, SPR biosensors have been widely applied in fundamental biological studies, drug discovery, affinity of bimolecular binding, clinical diagnosis, and environmental science and agriculture. The surface plasmon resonance (SPR) sensor as a surface sensing detection method has been applied in bio-applications for a long time due to its advantages, such as the simple, low-cost, rapid, real-time monitoring, label-free detection, revealing the binding kinetics of patient antibodies.[111,112] The SPR biosensing platform relies on changes in the localized refractive index (RI) of the sensing surface, which is caused by the binding between bio-probes and bio-analytes. In the SPR surface technique, the incident light can cause excitation of the charge density oscillation, which propagates along the interface between the metal–dielectric interface. To excite the SPR, the incident light has to satisfy the following condition:[113]

$$\frac{2\pi}{\lambda} n \sin\theta = \frac{2\pi}{\lambda}\left(\frac{\varepsilon_{mr} + {n_a}^2}{\varepsilon_{mr} + {n_a}^2}\right)^{1/2} \quad (1)$$

where ε_{mr} is the real part of the dielectric constant of the metal, n is the refractive index of the metal, n_a is the refractive index of the sensing medium, and θ is the angle of incident light. When the analyte flows through the surface of the SPR biosensor, the refractive index of the metallic surface changes, resulting in a change of excitation conditions. To re-excite the SPR, normally, the wavelength or incident light angle of the excitation light needs to be realigned. Based on such physical principles, the incident light intensity-dependent, incident light angle-dependent, or resonance light-phase SPR biosensors have been designed and applied. For the angle modulation SPR biosensor, the wavelength of the incident light source is fixed. With the changing of the dielectric constant of the measured medium, the resonance angle will shift.[114–116] The angle modulation SPR biosensor possesses the advantage of a simple structure and cheap optical–electrical units. However, it relies on high-quality angle modulation devices and low capability in real-time monitoring. The architecture of intensity-modulated SPR biosensors is the same as angle modulation SPR biosensors. The reflected light intensity is collected, which is related to the RI change of analytes. This type is simple and easy to measure, but the signal-to-noise ratio is relatively low, and it is easily disturbed by light source fluctuations and environmental changes.[117–119] For the wavelength-modulated SPR biosensor, a white light source is commonly used. The SPR spectrum was obtained by using a spectrometer, which shows the intensity of the reflected light with a minimum at the resonance wavelength. A small change in the refractive index of the analyte near the sensing surface can cause a significant shift in the resonant wavelength in the SPR spectrum.[120–123] Phase modulation SPR biosensors measure the phase characteristics of the light reflected under the condition of surface plasmon resonance. When the refractive index of the measured medium changes, the phase of the spectrum obtained by the spectrometer will also change accordingly. The phase modulation SPR biosensors can measure small shifts in the phase of light in the plasmon resonance region, which is derived by windowed Fourier transform,[124–126] and the detection limit can be improved by two orders of magnitude compared to angle modulation and wavelength modulation. In comparison with measuring the light intensity and wavelength, the phase is much more stable. The only disadvantage of the phase modulation SPR biosensors

is a complex setup that requires good knowledge to select the proper optic units.

In comparison to a planar Au film, the metallic nanostructure illustrates a higher performance. The metallic nanostructures (such as Au and Ag NPs) possess plasmonic properties of strong and controllable optical signal enhancement, and manipulation capabilities.[111] By proper design of the morphology of the metallic nanostructures, the SPR wavelength can be determined at a certain wavelength, which could improve the sensitivity of the SPR biosensors.[131,132] In a study by Guangyu Qiu,[127] the dual-functional plasmonic photothermal biosensor was applied in detecting the SARS-CoV-2 RNA sequence (Fig. 6a). Two-dimensional gold nanoscale islands (AuNIs) functionalized with DNA complementary receptors formed the sensing interface. The DNA reporter with specific DNA sequences can interact with SARS-CoV-2 RNA through nucleic acid hybridization. A microfluidic chip integrated with the sensing surface was designed as the detection chip. During the detection process, an external laser was applied to heat the sensing surface, which was induced by the plasmonic photothermal (PPT) effect of AuNIs and the calculated temperature of around 41 °C. Using two different angles of incidence, the plasmonic resonances of PPT and LSPR can be excited at two different wavelengths, which increased the stability, sensitivity, and reliability of the detection. By applying the PPT effect in SPR, the kinetics of DNA hybridization was largely increased, which decreased the binding time. The SPR biosensor responsible sensitivity also increased and the LOD was 0.22 pM.

To improve the sensitivity, another way is to increase the "mass" of analytes by designing sandwich structures that largely change the RI of the sensing surface. Normally, the Au NPs modified with a bio-probe are applied as the top materials to bind to the analytes, which have been bound to the sensing surface. In the architecture of the sandwich structure, Au NPs play two functions: (1) the localized plasmon effects between Au NPs and the Au film can enlarge the changes of resonance wavelength. (2) The Au NPs bounded to the sensing surface can make a bigger mass change, resulting in a larger RI change. By applying the sandwich structure, the detection limits for detecting the SARS-CoV-2 RAN sequence[128] (Fig. 6b), N protein[129] (Fig. 6c), and S protein[130] (Fig. 6d) are improved.

In comparison with the most common ATR structure, the SPR biosensor based on fiber optic surface plasmon resonance (FO-SPR) is also widely applied in bio-detection. In the FO-SPR sensor, the light propagates along with the optic fiber through total internal reflection. For each reflection, the evanescent wave is generated, which can excite the Au film and generate the surface plasma to propagate along with the Au film. With changing the surface complexes on the Au film, the exciting light wavelength intensity is changing or the excitation light wavelength should be optimized. The exposure sensing surface of FO-SPR can be directly put into the analyte's solution with the out-coupling of microfluidics channels. Moreover, the light is restrained in the optic fiber, which reduces the complexity of the alignment of the optic path. These properties make the FO-SPR an easy-to-fabricate device with high stability and good sensitivities. Jia-Huan Qu[112] designed a fiber-optic surface plasmon resonance (FO-SPR) biosensor in detecting anti-SARS-CoV-2 antibodies (Fig. 7a). This sensor greatly reduces the detection time-to-result of only 30 min compared to the conventional ELISA, and with enormous potential towards other applications in need of antibody quantification and

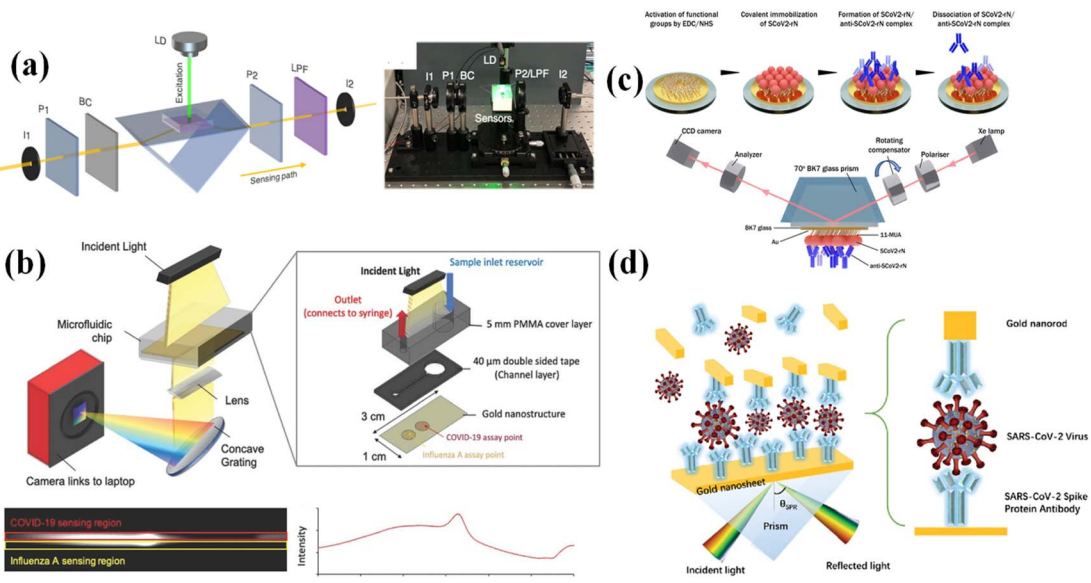

Fig. 6 (a) Schematic and experimental setup of the dual-functional PPT-enhanced LSPR biosensing system. Reproduced with permission from ref. 127. (b) Scheme of the SPR spectral imaging platform integrated with a microfluidic chip. A typical spectral image is shown, and it was obtained from the CCD. Reproduced with permission from ref. 128. (c) Schematic representation of the gold-coated sensor disk (Au-disk) surface modified with antigen SCoV2-rN, which was applied as an interactive surface. Reproduced with permission from ref. 129. (d) The SPR biosensor was designed using a sandwich structure. Reproduced with permission from ref. 130.

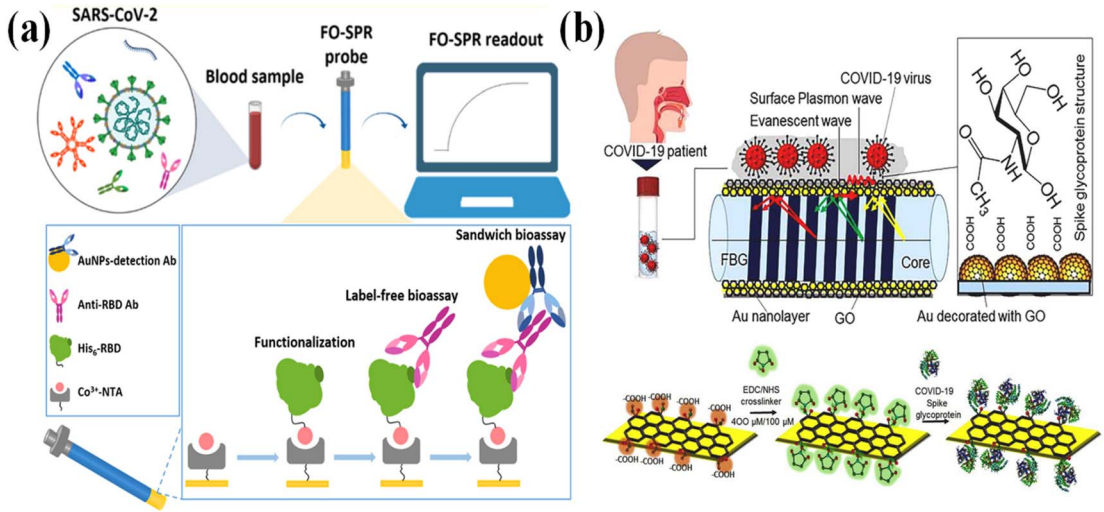

Fig. 7 (a) Schematic illustration of the FO-SPR biosensor for the detection of anti-SARS-CoV-2 antibodies in label-free samples, and the detecting mechanism using sandwich formats. Reproduced with permission from ref. 112. (b) Sensing mechanism diagram of the interactive surface of FO-SPR biosensor and the process of binding the spike glycoprotein of COVID-19 virus with activated GO. Reproduced with permission from ref. 133.

kinetic profiling. Alireza Samavati[133] used graphene oxide/Au/fiber Bragg grating (FBG) as a sensing interface in detecting the SARS-CoV-2 S protein in the saliva sample (Fig. 7b). This FBG probe can quickly detect COVID-19 within 10 s.

The SPR sensor has the great advantage of commercially-available systems and supporting facilities. However, for efficient SARS-CoV-2 detection, SPR faces several severe issues to resolve. First, the detection surrounding should be stable, especially for the temperature. Second, for the detection mechanism by SPR, interference of SARS-CoV-2 detection by SPR easily occurs by impurities in the solution, which reduces its specificity. The complexity of real samples needs to be minimized or eliminated by signal processing.

5. Field-effect transistors (FETs)

The FET biosensor is a label-free, highly sensitive, fast, and low-cost detection method.[134] By combining it with kinds of bio-probe and advanced functional nanomaterials,[135] FET biosensors have been applied in detecting various bio-molecules and diagnostic diseases.[136] Through screening the readable and amplified electrical signals, which are generated through an interaction between target bio-molecules and bio-probe on the sensing interface, the FET-biosensor can real-time monitor the detection process.[137,138]

Graphene is the most used channel material in FET. Graphene as an atomic thickness two-dimensional(2D) material has been regarded as the most renowned material.[140–143] The near ballistic transport and high level of mobility[143–145] of graphene make it an attractive platform for nanoelectronics applications,[146,147] particularly for high-frequency applications. Due to the scalability of graphene, devices achieve 2D atomic dimensions.[148,149] In addition, its optical and mechanical properties are ideal for micro/nano-mechanical systems, thin film transistors, transparent and conducting electrodes, and photonics.[150,151] Graphene is a gapless semimetal with zero overlap between its conduction band and its valence band. At room temperature, graphene demonstrates a strong ambipolar electric field effect and possesses high carrier mobilities of $\sim 1 \times 10^4$ cm^2 V^{-1} s^{-1}.[152] For the suspended graphene, its mobility can approach 2×10^5 cm^2 V^{-1} s^{-1} at a low temperature.[153] In the past decades, the graphene-based field-effect transistor (G-FET) biosensors were widely applied in the detection and diagnosis of diseases, such as Ebola virus,[154] heart failure,[155] human immunodeficiency virus (HIV),[156] cancer,[157] and viral exosomes in cells.[158] Giwan Seo[139] designed a graphene-based FET biosensor, and applied it in the real-time detection of SARS-CoV-2 (Fig. 8a) with a LOD of 242 copies/mL. This FET biosensor could detect the SARS-CoV-2 spike protein at concentrations of 1 fg mL^{-1} in phosphate-buffered saline and 100 fg mL^{-1} in clinical transport medium. Michael Taeyoung Hwang[159] used a liquid top-gated graphene FET biosensor with SARS-CoV-2 antigens with a LOD of 1 aM. Jiahao Li[31] applied reduced graphene oxide-FET in the detection of SARS-CoV-2 RAN with an LOD of 0.37 fM in 2 min. In the study of Jiahao Li,[31] the RGO-FET was applied in detecting SARS-CoV-2 RAN. The RGO solution was drop-casted on the FET channel, and the AuNP functionalized with complementary phosphonodiamidite morpholino oligos (PMO) probe was decorated on RGO to form a detection surface (Fig. 8b). The RGO-FET was applied in detecting RNA-dependent RNA polymerase (RdRP) in PBS, throat swab, and serum with the LODs of 0.37, 2.29, and 3.99 fM, respectively. The RGO-FET also was applied in detecting clinical samples in 2 min. A similar study was also performed by Esteban Piccinini.[160] He used the RGO-FET with a coplanar Ag/AgCl gate in the detection of the SARS-CoV-2 S protein with an LOD of 0.74 nM.

Except for carbon-based 2D materials, one-dimensional carbon nanotubes (CNTs) based on FET have been widely

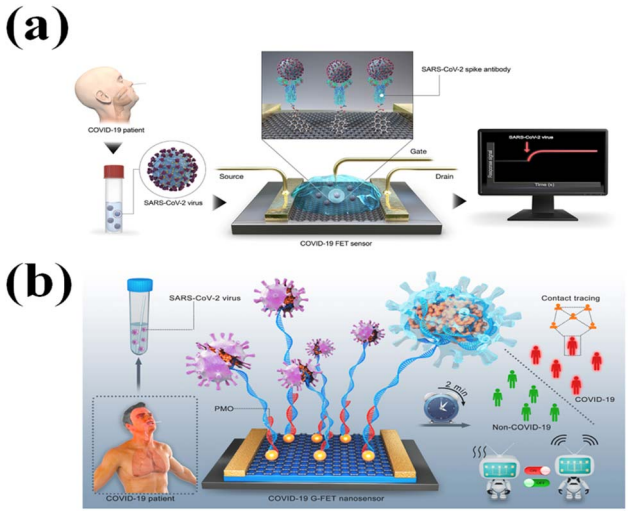

Fig. 8 (a) Schematic diagram of the COVID-19 FET sensor operation procedure. Graphene is chosen as the sensing material, and the SARS-CoV-2 spike antibody is conjugated on the graphene sheet through the i-pyrenebutyric acid ester *N*-hydroxysuccinimide, which is an interfacing molecule as a probing linker. Reproduced with permission from ref. 139. (b) Schematic diagram of the PCR-free rapid direct identification of COVID-19 using the PMO-functionalized G-FET nanosensor. Reproduced with permission from ref. 31.

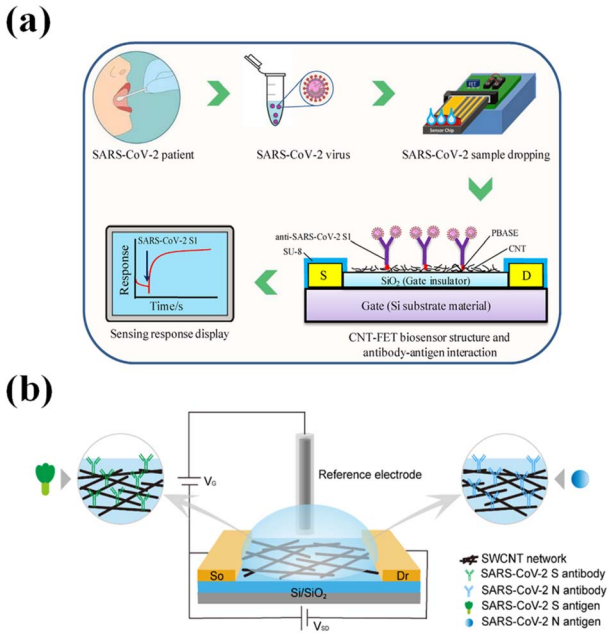

Fig. 9 (a) Schematic diagram of the CNT-FET biosensor for detecting the SARS-CoV-2 S protein. Reproduced with permission from ref. 161. (b) Schematic illustration of a liquid-gated SWCNT FET for the detection of SARS-CoV-2 SAg and NAg. Reproduced with permission from ref. 162.

studied in bio-detection. CNTs are molecular-scale wires with high mechanical stiffness and strength.[163] An SWNT with different chirality illustrates different electrical properties. It can be metallic, semiconducting, or semimetallic.[164] CNTs possess excellent electrical properties, good biocompatibility, and good size compatibility. These characteristics make it a good channel material to fabricate sensitive FET biosensors in detecting SARS-CoV-2.[163,165] Mazin A. Zamzami[161] designed a nanotube-based field-effect transistor in detecting SARS-CoV-2 S protein antigens. The single-wall carbon nanotubes (CNTS) with a length of 5–30 μm and a diameter of 1 to 2 nm were functionalized with the SARS-CoV-2 S protein antibody, which acts as a bio-probe to bind the SARS-CoV-2 S protein. The FET was fabricated on Si/SiO_2 substrates and designed using a backdated structure. The CNTs-FET can respond to the SARS-CoV-2 S protein diluted from 0.1 to 5000 fg mL^{-1}, and the LOD was 4.12 fg mL^{-1} of SARS-CoV-2 S protein in a 10 mM AA buffer solution (Fig. 9a). Wenting Shao[162] designed an SWCNTs-FET, in which the top gated structure was constructed by using a silver/silver chloride reference electrode (Fig. 9b). The SWCNTs modified by anti-SARS-CoV-2 S protein antibody were applied as a sensing interface. The LODs for detecting the S protein antigen and N antigen (NAg) were 0.55 fg mL^{-1} and 0.016 fg mL^{-1}, respectively. M. Thanihaichelvan[166] used a top-gated CNT-FET in detecting the target sequence of the SARS-CoV-2 virus. The gate electrode is the Ag/AgCl electrode, and the CNT functionalized with probe oligonucleotide was used as the sending interface. The detection limit for the oligonucleotide is 10 fM.

Except for graphene, 2D semiconducting materials hold great promise in the detection of biomolecules with higher sensitivity due to their tunable bandgap and the high surface-to-volume ratio.[169] In the 2D materials domain, transition metal dichalcogenides (TMDs) attracted much attention in designing TMDs FET-biosensor due to their direct bandgap, biocompatibility, and high mobility.[170] Molybdenum disulfide (MoS_2) as a new type of 2D layered transition metal dichalcogenides has been widely applied in FET. MoS_2 possesses lots of unique electronic, optical, and mechanical properties. Unlike the electric properties of graphene,[171,172] MoS_2 is a semiconductor with both the top and bottom surface of the Mo atoms layer bonded by the sulfur atoms to generate a covalent Mo–S band with the polarity in the vertical direction to the surface.[173,174] Junqing Wei[167] designed a MoS_2-FET in detecting antibodies using the SARS-CoV-2 S protein receptor in vaccinated serum specimens (Fig. 10a). The MoS_2-FET can quantitively detect the IgG within the range of 10^{-3} to 10^{-9} mg mL^{-1}.

Like single-layer MoS_2, WSe_2 as a TMD material is a direct bandgap semiconductor with bandgaps (E_g) between 1.2–1.8 eV.[175] WSe_2 films have pristine surfaces free of dangling bonds that can reduce surface roughness scattering, and lead to high mobility.[176] The free dangling bonds also reduce interface traps, and result in a low density of interface states on the semiconductor–dielectric interface.[176] Parvin Fathi-Hafshejani[168] designed and fabricated a WSe2-based FET, and it was applied to detect the SARS-CoV-2 virus with a LOD of 25 fg μL^{-1} (Fig. 10b).

The FET detection of SARS-CoV-2 can achieve high sensitivity, but the selectivity is relatively low. The challenge for the FET SARS-CoV-2 sensor is to achieve highly selective recognition. For FETs, the electrical signal changes induced by bio-

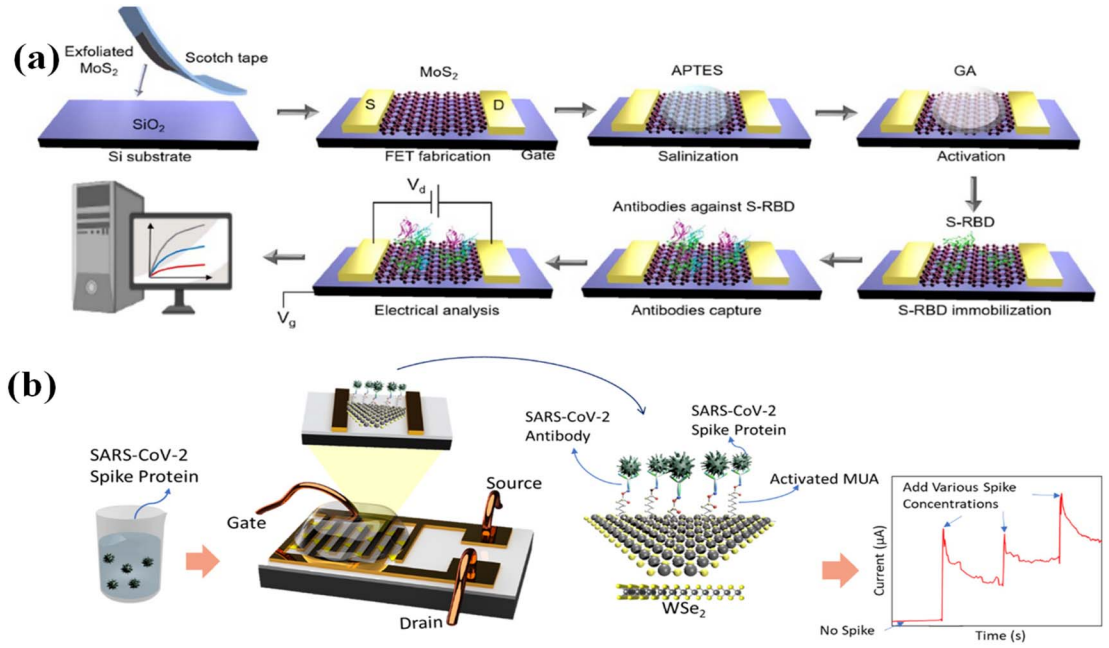

Fig. 10 (a) The schematic of the MoS_2-FET fabrication, functionalization, and its application for antibodies against S protein detection. Reproduced with permission from ref. 167. (b) Schematic diagram of the fabricated monolayer WSe_2-based SARS-CoV-2 FET biosensor. Reproduced with permission from ref. 168.

interfaces need to be screened by stable control samples, and some fake electrical signals should be carefully identified. Another problem is the re-utilization of the FET SARS-CoV-2 sensor. The regeneration of SARS-CoV-2 bio-interfaces may be complicated for FETs construction. The reliable regeneration of the FET SARS-CoV-2 nano-biosensor needs more investigation.

6. Fluorescence

Fluorescence spectroscopy is a powerful identification technique and images the emitters with ultra-high sensitivity, and its LOD reaches the single molecule level.[177] Fluorescence-based sensing techniques possess advantages, such as high speed, easy operation, good sensitivity, real-time motoring, good biocompatibility, and noninvasive characteristics.[178,179] Fluorescence biosensors are the most popular optic devices, and they have been widely studied and used in bio-detection and disease diagnosis.[180–182] Fluorescence biosensors can directly provide the readout of bio-analytes or bio-interaction information that is located or occurs in different biological organisms and living cells.[183]

The most common fluorescence biosensors are based on metal-enhanced fluorescence or plasmon-enhanced fluorescence. Metallic nanostructures can generate localized surface plasmon, which can excite the fluorophore near the metallic nanostructures more efficiently and increase the decay rate, resulting in stronger fluorescence.[188,189] The enhancement of the fluorescence can be affected by several factors, such as the morphology of metallic NPs, the distance between the fluorophore and the NPs, the quantum yield of fluorophores, as well as the spectral overlap between SPR and excitation/emission spectra of the fluorophores.[189] A grating-coupled fluorescent plasmonic (GC-FP) was studied in detecting SARS-CoV-2 by Nathaniel C. Cady[184] (Fig. 11a). The sensing interface was a gold-coated nanoscale grating, and the SARS-CoV-2 antigens or control proteins were sprinted with an array of 400 μm diameter spots. The Alexa Fluor 647 tagged anti-human IgG was applied to enhance the detection fluorescence intensity. This fluorescence-enhanced biosensor can simultaneously detect the antibody levels for multiple antigens using one sample, and the maximum measuring time was 27 min. The GC-FP biosensor possesses a selectivity of 100%. In comparison with the fluorescence biosensors based on a single signal change, the radiometric fluorescence biosensors are more attractive. Förster resonance energy transfer (FRET) is a good choice to design a radiometric fluorescence biosensor. FRET is a non-radiative physical process, in which the donor is excited by extra energy, and then transfers its energy to an acceptor proximal to the ground state *via* long-range dipole–dipole interactions.[190] The molecular chromophore that offers the energy is regarded as a donor (D), and the molecular chromophore that accepts the energy is considered an acceptor (A). The donor chromophore, originally in the ground state, is transferred by absorbing an external photon into an excited state. Its energy is transferred to the acceptor through the nonradiative process of energy transfer from dipole to dipole, thus being transferred back to the ground state. There is also a competing process that exists. The excited photons in acceptors and donors both can lose energy to the ground state by emitting fluorescence. During the FRET process, several requirements must be satisfied. Firstly, adequate spectral overlap between the excitation of the acceptor and the emission of the donor should exist. Secondly, the FRET

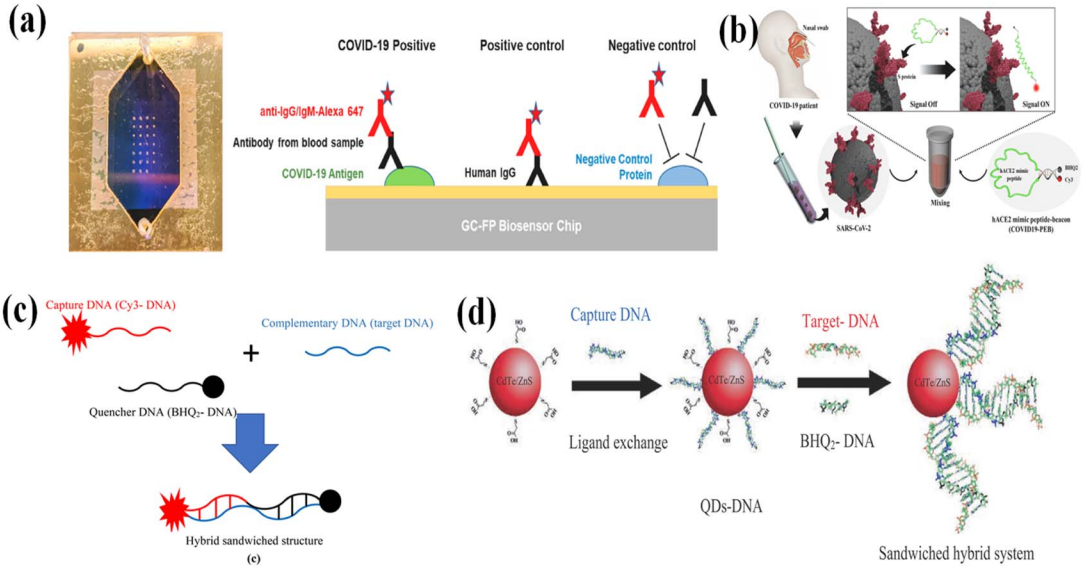

Fig. 11 (a) Immunosensing mechanism of S-IgG detection using an optofluidic pointing-of-care testing platform (POCT) and a typical fluorescence signal trace for S-IgG detection. Reproduced with permission from ref. 184. (b) Schematic illustration of the simple detection method of SARS-CoV-2 using the hACE2 mimic peptide-based molecular beacon (COVID 19-PEB). Reproduced with permission from ref. 185. (c) A schematic representation for pairing different DNA single strands (containing Cy3-DNA, BHQ 2-DNA, and complementary DNA) to form a hybrid sandwiched structure. Reproduced with permission from ref. 186. (d) A schematic of the DNA-conjugated CdTe/ZnS QDs nanoprobe for the detection of complementary (target-DNA) derived from the COVID-19 virus genome. Reproduced with permission from ref. 187.

process is efficiently affected by the distance between donor and acceptor. The FRET efficiency is inversely associated with the sixth power of the distance between the donor and the acceptor. For such reason, the distance between the donor and acceptor should be within a range of 10 nm.[191–195] Thirdly, for the dipole–dipole interaction, at least one donor and acceptor should possess a certain degree of rapid rotational freedom to obtain favorable energy transfer orientation. When all of these conditions are satisfied, the excited electrons in the donor have a possible competing pathway to transfer their energy to the acceptor, instead of emitting energy as fluorescence. For the fluorescence biosensors, two elements are required, which are the recognition element and a reporter.[196] The recognition element is responsible for selectively binding to the analyte, while the reporter can generate the signal. When the recognition element combines with the analyte, the fluorescence signal that comes from the reporter could be quenched[197] or enhanced[198] fluorescence. Byunghoon Kang[185] developed an ACE2 mimic peptide beacon (COVID-19-PEB) for the simple detection of SARS-CoV-2 using a FRET system (Fig. 11b). The COVID-19-PEB can specifically bind to the S protein RBD of the SARS-CoV-2. In the absence of the SARS-CoV-2, the COVID-19-PEB is a form of a hairpin structure, in which the fluorescence signal is minimum due to the FRET process between the BHQ2 (as acceptor) and Cy3 (as donor). Under the condition of the existence of ARS-CoV-2, the hairpin structure of COVID-19-PEB is open, resulting in an increase in the fluorescence signal within a short period. The LOD of this method is 52.5 pM. Ghasem Rezanejade Bardajee[186] designed a FRET pair, where the BHQ2 was applied as an acceptor and Cy3 was applied as a donor in detecting the specific RAN sequence of the SARS-CoV-2 (Fig. 11c). The complementary sequence of the target SARS-CoV-2 sequence was divided into two parts. One part is modified with Cy3 organic dye, and another part was functionalized with BHQ2. In the absence of a complementary sequence, the FRET occurred. In the presence of the complementary sequence, the efficiency of the FRET was blocked, resulting in the fluorescence intensity decrease. Through such a design, the LOD is 0.0995 μM. He[187] used CdTe/ZnS QDs as a donor and BHQ2 as an acceptor (Fig. 11d). By properly designing the CdTe/ZnS-DNA and BHQ2-DNA structures, the sandwich structure (CdTe/ZnS-DNA)-(target SARS-CoV-2 RNA)-(sequence-DNA) was formed, in which the FRET between the CdTe/ZnS and BHQ2 occurred. By adjusting the on/off of the FRET process, the target SARS-CoV-2 RNA sequence was detected with an LOD of 0.000823 μM.

Fluorescence methods have the advantage of direct low-cost identification with highly commercially-available detection systems. However, fluorescent SARS-CoV-2 sensors are affected by the detection conditions. The modification of the labeled bioprobes is complicated, and the fluorescence intensity can be affected by several factors. Therefore, the fabrication of reliable and easily fabricated fluorophore label bioprobes needs to be further studied.

7. Electrochemistry

Electrochemical transducers possess the characteristics of cost efficiency, simplicity, high selectivity, and high sensitivity.[199] The electrochemical sensors have been applied in detecting various viruses, such as Hepatitis B virus,[200] Ebola virus,[201] HIV,[202] Hantavirus,[203] and Epstein–Barr virus[204] with excellent

sensitivities. Electrochemical biosensors are a combination of electroanalytical methods and bio-interaction, which occurs between the bio-probes and the target analytes. The bio-probes are responsible for identifying and binding to the analytes, and the electroanalytical event plays a role in generating electrochemical signals, which is monitored by a transducer that is related to the analyte concentration. There are mainly two kinds of electrochemical biosensors that are biocatalytic devices and affinity sensors.[205] For biocatalytic devices, enzyme electrodes are applied to identify target analytes such as glucose, lactose, and xanthine and produce electroactive species. For the affinity sensors, the electrodes functionalized with the bio-probes are utilized to selectively bind to the analyte, such as an antibody, nucleic acid, or receptors. The most used affinity sensors in biology are based on immunosensors, where the antigen or hapten are detected by using antibodies as bio-probes. The electrochemical transducer transfers the binding event into a readable electrical signal. The RNA/DNA affinity sensors also play an important role in medical diagnostics, cancers detections, viral infections, and genetic diseases, where the complementary nucleic acid sequence is applied as a probe to identify the target nucleic acid sequence.

In the electrochemical techniques, the current, potential, and impedance are the main measurable parameters, in which the voltammetry technique, impedance technique, conductometry technique, and potentiometry technique are applied.[209] The voltammetric technique measures the current changes between the working electrode reference electrode and reference electrode by applying a potential. Electrolysis is the result of the current using an electrochemical reduction or oxidation at the working electrode. Electrolysis currents are limited by the mass transport rate of the molecules toward the electrode. The current is a reflection of the electrochemical reduction or oxidation at the working electrode. When a scanning voltage is applied, the current response is a spike that is proportional to the analyte concentration. Voltametric methods include linear sweep voltammetry (LSV), cyclic voltammetry (CV), differential pulse voltammetry (DPV) and square-wave voltammetry (SWV).[210] Lokman Liv[206] used a CV platform to detect SARS-CoV-2 spike antibodies in saliva and oropharyngeal

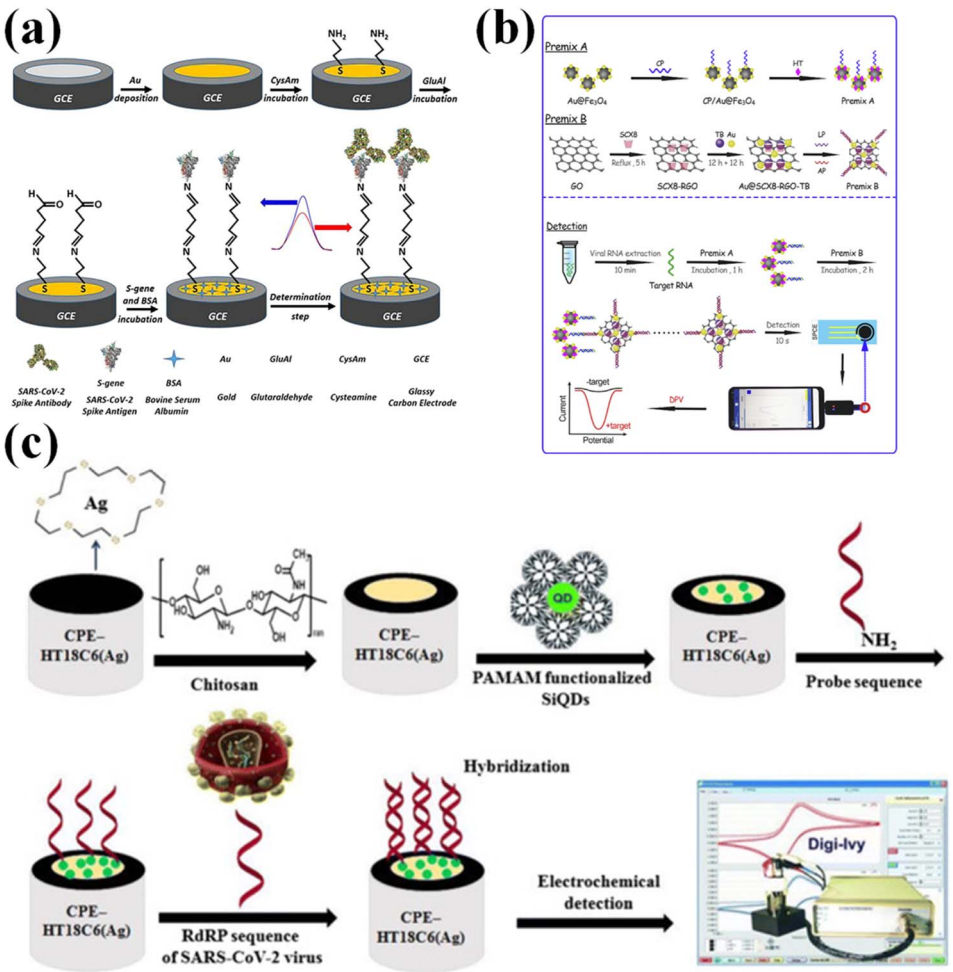

Fig. 12 (a) Schematic representation of SARS-CoV-2 detection using the electrochemical biosensor. Schematic illustration of the fabrication process of an electrochemical genosensor. Adapted with permission from ref. 206. (b) Preparation of a premixed A and B, and the detecting process by using electrochemical methods equipped with a smartphone. Adapted with permission from ref. 207. (c) Schematic illustration of the fabrication process of an electrochemical genosensor. Adapted with permission from ref. 208.

swab samples (Fig. 12a). The glassy carbon electrode (GCE) was applied as the working electrode, and the BSA/S-gene/GluAl/CysAm/Au/GCE (BSA: bovine serum albumin, S-gene: SARS-CoV-2 antigen, GluAl: glutaraldehyde, CysAm: cysteamine) complex was applied as a sensing surface. With the presence of the SARS-CoV-2 spike antibody sample, the scan peak height decreased due to the large size of the immuno-complex to block the electron transfer. The proposed method illustrated a linear response to the SARS-CoV-2 spike antibody in synthetic media and saliva/oropharyngeal swab samples varied from 0.1 to 1000 ag mL^{-1}, and the LOD was 0.01 ag mL^{-1}. Differential pulse voltammetry (DVP) is a very sensitive technique owing to its low capacitive current.[211,212] In DVP, short pulses with small amplitude are superimposed on a linear ramp, and enhanced discrimination of faradaic currents is measured before and after applying the pulse.[213] By analyzing the relationship between the potentials and the current difference of each pulse, the potentials of the envisaged oxidation or reduction reaction can be calculated.[214] Hui Zhao[207] applied a super sandwich-type recognition strategy in detecting RNA of SARS-CoV-2 by using portable electrochemical smartphone equipment with differential pulse voltammetry (DPV) (Fig. 12b). The probe nucleic acid sequence was functionalized with Au@Fe_3O_4, and it was applied to bind the target ssDNA. The total structure of nucleic acid@Au@Fe_3O_4 was named premix A. The premix B was a host–guest complex that was Au@SCX8-TB-RGO-(labeled signal obe) acting as a bioconjugate. The premix A, premix B, and SARS-CoV-2 target sequence form a sandwich structure, which illustrates a strong DPV signal with a LOD of 200 copies mL. Leila Farzin[208] developed an early diagnosis of RNA of SARS-CoV-2 by using DPV methods (Fig. 12c). The CPE–HT18C6(Ag)/chitosan/SiQDs@PAMAM/probe (CPE: carbon paste electrode, HT18C6: hexathia-18-crown-6, SiQDs: Si quantum dots) sequence was applied in the detection of SARS-CoV-2 RdRP (RdRP: RNA-dependent RNA polymerase) sequence. The proposed nanosensor exhibited a wide linear range of detection, which was 1.0 pM–8.0 nM.

In electrochemical impedance spectroscopy (EIS) measurements, a small amplitude sinusoidal AC signal with different frequencies are applied at working electrodes. Upon changing the frequency of the AC, the ratio of the voltage to the current of the AC signal changes. A small change in the electrode surface can change the magnitude of the system impedance. Juan Carlos Abrego-Martinez[215] used EIS to detect the S protein of the SARS-CoV-2. The LOD was 66 pg mL^{-1} in 40 min. Jie Zeng[216] applied an impedimetric biosensor in detecting COVID-19 antibodies in serum. The gold micro-interdigitated electrodes were photolithographed on SiO_2. The SARS-CoV-2 S protein was functionalized between the Au electrodes with a channel length of 4 μm. With the assistance of AuNPs modified by antibodies, the LOD of detecting purified anti-S protein antibodies was 200 ng mL^{-1}. With the assistance of dielectrophoretic (DEP), the detection time was shortened to 30 min by sacrificing the LOD, which was 2 μg mL^{-1}.

For the architecture of electrochemical biosensors, a three-electrode system or a two-electrode system is widely applied, where the working electrode plays a pivotal role.[219,220] A typical three-electrode electrochemical cell is made up of a working electrode, a reference electrode, and an auxiliary electrode. Normally, the semiconducting and conducting materials can be used as working electrodes, such as carbon or platinum, that can be in various sizes ranging from bulk materials and nanostructures, which could affect the performance selectivity and sensitivity.[221] Normally, the reference electrodes and the auxiliary electrodes are Ag/AgCl and platinum wire, respectively. The two-electrode system consists of the working electrode and reference electrode under the condition of low current density. Normally, the two-electrode system is generally applied in disposable sensors because of their lower cost, and the long-time stability of the reference is not needed. In comparison with a two-electrode system, charge from electrolysis flows through the auxiliary electrode instead of the reference electrode, which protects the reference one from changing its half cell potential in a three-electrode system. Abdulhadee Yakoh[217] designed an electrochemical biosensor fabricated by using paper applied in the detection of SARS-CoV-2 antibodies and antigens (Fig. 13b). The test sheet consisted of 3 folding layers: a working ePAD, a counter ePAD, and a closing ePAD (Fig. 13a). The three-dimensional wax barrier was a printed pattern to isolate the hydrophilic center of each zone in which the solution could flow through to the working ePAD (Fig. 13c). The counter electrode (CE) and the reference electrode (RE) were printed and integrated on the counter ePAD. Through such architecture, a three-electrode system was established. The SARS-CoV-2 spike protein was modified on the test zone of the working ePAD. The paper-based electrochemical biosensor can detect the SARS-CoV-2 IgG and IgM in the range from 1 to 1000 ng mL^{-1} with LODs of 0.96 and 0.14 ng mL^{-1}, respectively. Razieh Salahandish[218] designed a dual working-electrodes immune-biosensor in detecting SARS-CoV-2 N-protein in spiked samples, in which the N protein antibodies are applied as bio-probes (Fig. 13d). The two working electrodes can simultaneously give the detecting results, which can corroborate each other (Fig. 13e). This biosensor can reach the LOD of 56 fg mL^{-1} and the detection time is 1.5 min.

For the electrochemical biosensors, the bio-probes play important roles in biosensing. Genxi Li and his research team have made great progress in designing electrochemical biosensors combined with kinds of bio-probes that have been applied in detecting SARS-CoV-2 viruses. In his study, signal amplification was applied, and it proves that the terminal deoxynucleotidyl transferase catalyzes the hairpin assembly (CHA) with amplificated electrochemical signals. By using this method, the LOD for detecting SARS-CoV-2 RNA,[222] the N genes and the RdRp genes[223] were 26 fM and 57 fM, respectively. He also proposed an electrochemical biosensor for the detection of SARS-CoV-2 based on the aid of the target-triggered cascade signal amplification strategy. This method possessed a LOD of 45 fM in detecting ssDNA of SARS-CoV-2, with a broad linear range between 0.1 pM and 3000 pM.[224] Except for the common RNA or antibody detection, he came up with a new method that used papain-like cysteine protease (PLpro) as a biomarker in detecting SARS-CoV-2, which can be used in real surroundings, including blood and saliva with a LOD of 27.18 fM.[225]

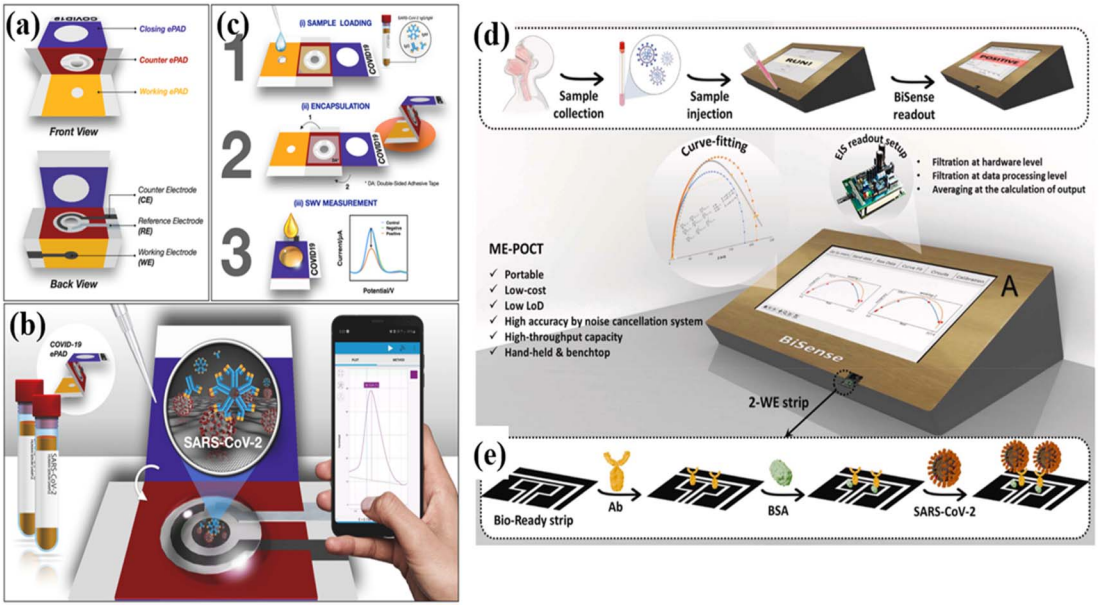

Fig. 13 Schematic illustration of the (a) device components, (b) detection principle, and (c) detection procedure of the COVID-19 ePAD. Adapted with permission from ref. 217. (d) Schematic illustration of detecting SARS-CoV-2 by using the proposed two-working electrode electrochemistry biosensors. (e) Two-working electrode strip with a carboxyl-rich surface ready to be immobilized for direct antibody (Ab) immobilization, followed by surface blockage using bovine serum albumin (BSA) for ultimate SARS-CoV-2 virus conjugation in clinical specimens. Adapted with permission from ref. 218.

Electrochemical SARS-CoV-2 sensors have the advantage of low-cost and commercially available systems. They can also achieve high sensitivity by using carefully designed sensing bio-interfaces. The challenges for electrochemical SARS-CoV-2 sensors remain in the repeatable quantified detection. For electrochemical detection, the detection process needs to be done in a three-electrode system in the electrolyte. Many environmental impurities may influence the electrochemical detection system, including potential, bio-interfaces or reference electrode stability. Therefore, a stable and robust electrochemical detection system should be designed to achieve repeatable quantified detection with high sensitivity and selectivity at the same time.

8. CRISPR-Cas and Argonaute

CRISPR-Cas[226–228] and Argonaute[229–231] systems are deemed as the next-generation diagnostic technology, as excellent gene editing tools. In particular, CRISPR-Cas12a and CRISPR-Cas13a have attracted interest due to their highly accurate gene-editing capabilities and crosscutting activities.[232] CRISPR-Cas-based and Argonaute-based SARS-CoV-2 detection methods are more specific, convenient, and reliable. Cas12 and Cas13 as RNA-directed CRISPR-related proteins can be programmed to detect specific DNA and RNA sequences from pathogens with single-base pair specificity, respectively.[226,233,234] Ma *et al.* designed the CRISPR-Cas12a powered SERS bioassay for SARS-CoV-2 detection with a LOD of 1.9 copies per mL.[235] Ashwin Ramachandran *et al.* constructed a selective ionic focusing technique assistant CRISPR assay method in detecting SARS-CoV-2 RNA in 35 min. The assay was performed in a microfluidic channel, in which the electric field control was used to accelerate the CRISPR assay by cofocusing Cas12–gRNA reporters, and targets.[228]

Argonaute is a nucleic acid-oriented endonuclease that prefers to be guided by short 5′-phosphorylated single-stranded DNA and cuts DNA substrates in the absence of a proto-spatial adjacent motifs (PAM). The selection of target DNA cleavage sites is not subject to specific sequence restrictions. Wang *et al.* proposed a method called PLCR (Pyrococcus furiosus Argonaute coupled with modified Ligase Chain Reaction), and applied this technique to nucleic acid detection. In this method, the PfAgo (Pyrococcus furiosus Argonaute) was applied to specifically cleave DNA and LCR to precisely distinguish single-base mismatch, where the PfAgo can only cleave target DNA guided by phosphorylated DNA guides longer than 14-mer. By utilizing this technique in other coronaviruses and multiplexed detection, it effectively reduced the detection time to less than 70 minutes.[230] Similar work also has been done by Wang *et al.*, in which PfAgo mediated nucleic acid detection method can significantly reduce the time of detecting COVID-19.[236] Ye *et al.* developed a multiplex Argonaute (Ago)-based nucleic acid detection system (MULAN), which was applied in RNA detection. The advantage of MULAN is that it possessed a detection resolution of a single base, which illustrated good performance in detecting mutant genotyping with a LOD of five copies per reaction.[231]

In summary, biosensing based on CRISPR-Cas and Argonaute proteins represents a conceptually novel paradigm for virus detection. Due to their unique biocharacters, they can be

independently used to detect viruses with excellent sensitivity. The more important aspect is that they can be integrated with some existing methods to suit diverse needs, such as being coupled to fluorimeters,[232] FETS,[237] SERS,[235] and electrochemical biosensors.[226] These combinations have attracted researchers' interest, and have great potential in nucleic acid detection with high specificity and sensitivity.

9. Colorimetric biosensor

The colorimetric biosensor is an excellent inspection technology because it is sensitive, simple, rapid, and inexpensive. Colorimetric biosensors can rapidly detect SARS-CoV-2, especially in resource-limited regions, where external devices and reagents are not needed.[238] The colorimetric detection technique is capable of providing results that are visible to the human eye. The miniature devices based on the colorimetric technique are popular because they are user-friendly, and they can capture images *via* electronic benchtops, as well as wearable devices. By applying nanomaterials, it can dramatically amplify the signal intensity of colorimetric biosensors and improve the sensitivity of biological target molecules.[239] Gold nanoparticles (AuNPs) are widely used in biomedical colorimetric assays because they are simple to produce and physically stable. AuNPs exhibit a unique optoelectronic feature where the chromogenic effect is caused by the aggregation of the AuNPs.[240] Karakus *et al.* developed a simple and selective AuNP-based biosensing platform that enables the colorimetric detection of the SARS-CoV-2 spike antigen at the level of 1 ng mL^{-1}. Karakus *et al.* used the color change phenomenon caused by the rapid and irreversible aggregation of AuNPs when the antibody interacts with the antigen. Through this method, the color change can be readily observed by eye, and its LOD was 48 ng mL^{-1}.[241] Some performance comparisons of the colorimetric biosensors are summarized in Table 1.

10. Mutation detection

SARS-CoV-2 has shown a strong capability for mutation, and various mutations dominate the epidemic at different periods in different countries. For detecting the mutation of SARS-CoV-2, the best way is to detect the RNA sequence of the SARS-CoV-2 virus. By identifying the existence of the mutated RNA sequences, the mutated SARS-CoV-2 can be detected. For the SERS, the base information located on the specific position of RNA can be detected, but it requires a special SERS substrate or special bio-probes. Lei Wu[249] designed a stem-loop structure that can specifically hybridize a perfectly matched DNA sequence and the mutated DNA sequence (Fig. 14a). The closed loop does show a SERS signal, while the open loop does not have a SERS signal. This design has been applied in identifying the mutated DNA sequence of cancer cells. Jian-An Huang[250] reported an approach to control the residence time of the DNA sequence through an Au hole (Fig. 14b). The DNA is absorbed in a single nanoparticle and passes through the Au hole, and the four DNA bases can be distinguished by analyzing the characteristic Raman peaks of the bases. Another method based on Raman spectroscopy in detecting the mutation of oligonucleotides is tip-enhanced Raman scattering (TERS). For TERS, the signals are mainly enhanced by the nanoscale gap between a silver tip and a metal substrate. Due to the small size of the tip, the TERS can resolve a single-stranded DNA/RNA molecule with a spatial resolution below 1 nm (Fig. 14c).[251,255,256] This extremely high resolution provides a possibility of figuring out the type of mutated base and its position. For detection of mutation by using SPR[127,128] (Fig. 15a–c), fluorescence methods[252,257] (Fig. 15d), FET[253] (Fig. 15e), and electrochemistry methods[254] (Fig. 15f), the kinetic of the hybridization can reveal the existence of a mutation. Because of the existence of mutated bases, the kinetic rate is changed, which can be monitored by measuring the hybridization signal intensity *vs.* hybridization time. However, these methods cannot specifically indicate where the mutated base is located.

11. Perspective

Table 2 illustrates the LOD and the detection time of biosensors applied in detecting SARS-CoV-2. All these biosensors have been applied to detect the real sample of the SARS-CoV-2 virus, and show good sensitivity and short detection time. The bio-probes such as ACE2, S protein antibody, and specific DNA sequences are selected to bind to the specific component of SARS-CoV-2. Among these biosensors, most of them rely on single optic or electric signal changes caused by the state changes on the sensing surface and the state changes, owing to bio-interaction between the probe and the target analyte. Consequently, the robust sample is always changing in identifying the SARS-CoV-2.

Table 1 Description of colorimetric biosensors for the detection of SARS-CoV-2

Nanomaterial	Biological recognition element	Target	LOD	Ref.
AuNPs	ssDNA	Gene N	10 copies per μL	242
Fe_3O_4/Au core–shell	Anti-spike protein antibodies	Protein spike	1200 PFU mL^{-1}	243
AuNPs	Antibody monoclonal (mAb)	Protein spike	48 ng mL^{-1}	241
AuNPs	Antigen	Protein N	150 ng mL^{-1}	244
AuNPs	Antibody rabbit IgG	Protein N	3 ng mL^{-1}	245
AuNPs-ACE2	ACE2 receptor	Protein spike	1.54×10^{-4} ng mL^{-1}	246
AuNPs-N	protein N-antigen	IgG, IgM eIgA		247
Polyurethane polydiacetylene	Anti-N protein	Protein spike		248

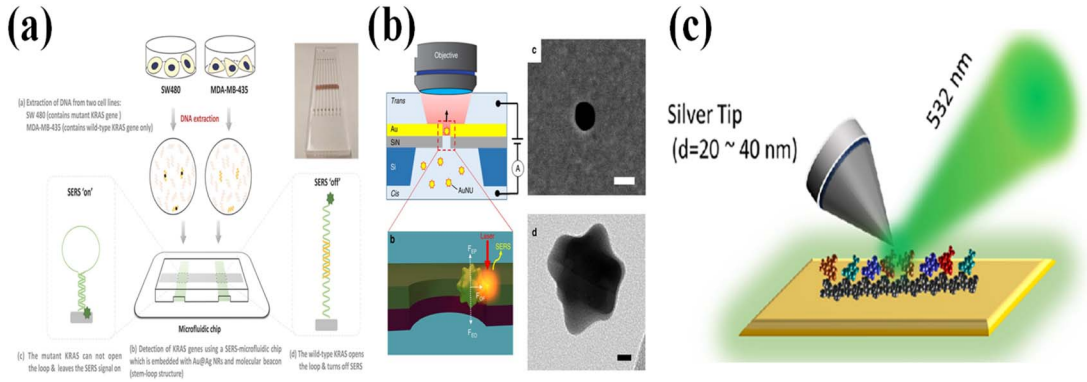

Fig. 14 (a) The microfluidic chip for SERS analysis of cellular DNA mutations. The NDA and mutated DNA pass through the microfluidic channel coated with Au@Ag NRs. The mutant KRAS sequences maintain the stem-loop structure, resulting in the 'SERS-on' state, while the KRAS is disrupted due to the hybridization of target sequences with the molecular beacon resulting in the 'SERS-off' state. Adapted with permission from ref. 249. (b) The diagram of trapping the single DNA passing through the Au nanohole. By controlling the resident time, the specific base information of DNA can be extracted by plasmon effects induced by the Au and nanoparticles. Adapted with permission from ref. 250. (c) Diagram of identifying the base in the DNA/RNA sequence by using TESR. Adapted with permission from ref. 251.

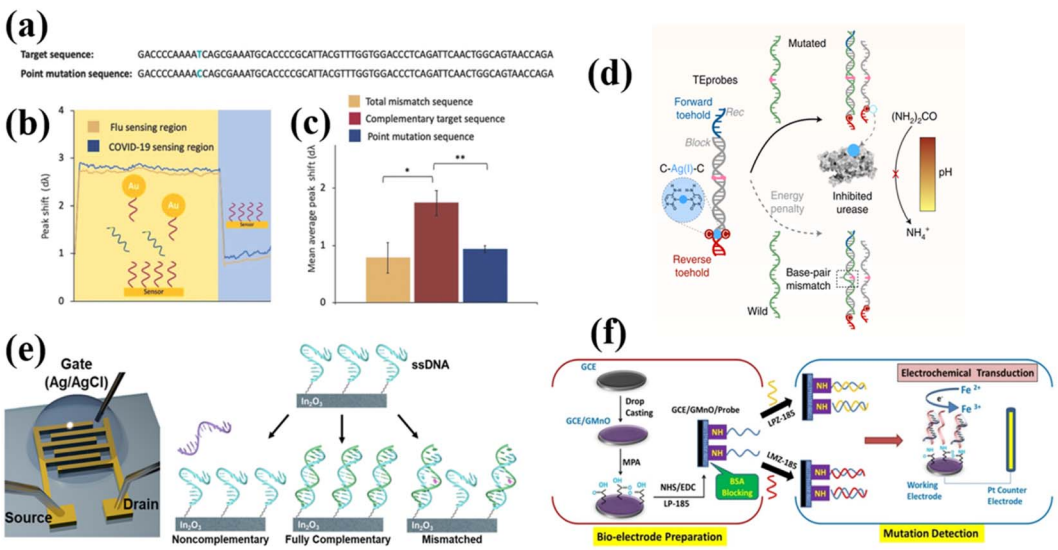

Fig. 15 (a) The target and single basepoint mutation mimicking sequences. (b) The result of detecting a target and a single base mutated COVID-19 sequence (100 fM) by using SPR methods. (c) The wavelength signal shifts in both sensing regions in response to the working solution. Adapted with permission from ref. 128. (d) To precisely control the net thermodynamic energy of the strand displacement reaction induced by input RNAs, a double stranded DNA probe is designed to tune its forward and reverse toehold terminal sequences. The difference between mutant and wild-type viral RNAs is the strand displacement reaction based on the thermodynamic energy penalty derived from a single base pair mismatch. Recognition of viral RNAs leads to the release of a urease inhibitor metal ion, Ag(I), and thus controls the cleavage of urea and the level of NH_4^+. We identify key mutation markers of SARS-CoV-2 variants, such as alpha, beta, gamma and delta, and visualize them using pH indicators. Adapted with permission from ref. 252. (e) The structure of the FET in detecting mutated oligonucleotide, and FET functionalized with ssDNA that is exposed to non-complementary, fully complementary, or mismatched sequences. Adapted with permission from ref. 253. (f) Schematic representation of the fabrication of the electrochemical sensing platform, and the response principle of detecting mutated target sequence. Adapted with permission from ref. 254.

SERS is an optic method with high accuracy because it reveals the finger print information of the molecules. During the SERS experiments, the characteristic peaks of the bio-probes and the target analytes can be observed. Due to the bio-interaction, the SERS intensity of the characteristic peaks of the probe can change or shift. By analyzing the appearance of the new peaks caused by the analytes and the changes in the probe SERS peaks, the existence of the SARS-CoV-2 can be detected. The SERS substrates are the key to enhanced Raman scattering. The chemically synthesized metallic nanostructures are applied in SERS, but the introduced chemical bond in synthesis always shows a strong fluorescence background or even a strong Raman signal. This unexpected optic matter highly affected SERS performance. Moreover, the repeatability

Table 2 The comparison of the different SARS-CoV-2 nano-biosensors

Methods	Analyte	LOD	Detection time	R^2 for the linear fit	Selectivity	Ref.
SERS	SARS-CoV-2 spike protein	1 fg mL^{-1}	15 min	0.9201		76
	SARS-CoV-2 spike protein	5×10^{-9} mol L^{-1}	—			77
	Breath volatile organic compounds (BVOCs)	—	5 min		96.2%	103
	SARS-CoV-2 virus in Crude water	255 copies per L	10 min	0.9688		78
	SARS-CoV-2 spike protein	0.77 fg mL^{-1}	4 h	0.99		79
	SARS-CoV-2-specific IgM/IgG antibodies	100 fg mL^{-1}	30 min			90
	IgM/IgG	1 pg mL^{-1}	25 minutes	0.99		84
	IgM/IgG	0.1 nm mL^{-1}	15 min			85
SPR	COVID-19 cDNA sequence	1 pM	3 min			127
	COVID-19 NA sequence	100 aM	Real-time			128
	SARS-CoV-2 N protein	85 fM	Real-time			258
	Anti-SARS-CoV-2 antibodies in whole blood samples	100 ng mL^{-1}	30 min	0.96		112
	SARS-CoV-2 in saliva	1.6 × 103 copies per mL	10 s			133
FET	SARS-CoV-2 antigen protein	1 fg mL^{-1} in buff	Real-time			139
	SARS-CoV-2 virus from clinical samples	242 copy per mL				
	SARS-CoV-2 RAN	0.37 fM	Within 2 min	0.997		31
	SARS-CoV-2 S protein antigens	4.12 fg mL^{-1}	Real-time		92%	161
	N antigen of SARS-CoV-2	0.016 fg mL^{-1}	Within 5 min			162
	RNA sequence of the SARS-CoV-2 virus	10 fM	Real-time			166
	SARS-CoV-2 S protein receptor	10^{-3} mg mL^{-1}	—			167
	SARS-CoV-2 virus	25 fg μL^{-1}	Real-time			168
Fluorescence	SARS-CoV-2 IgG antibodies	12.5 ng mL^{-1}	Within 7 min			259
	SARS-CoV-2 virus in serum	—	~30 min	0.998	100%	184
	SARS-CoV-2 virus	52.5 pM	1 h			185
	RAN sequence of the SARS-CoV-2	0.0995 μM	20 min	0.9945		186
	SARS-CoV-2 RNA	0.000823 μM	25 min	0.9825		187
Electrochemical	SARS-CoV-2 spike antibodies in saliva/ oropharyngeal swab	0.01 ag mL^{-1}	30 min	0.98		206
	RNA of SARS-CoV-2	200 copies per mL	3 h	0.999	High	207
	RNA of SARS-CoV-2	1.0 pM	25 min		High	208
	S Protein of the SARS-CoV-2	66 pg mL^{-1}	40 min	0.9954	42.5%	215
	SARS-CoV-2 S protein	200 ng mL^{-1}	30 min	0.999		216
	SARS-CoV-2 IgG and IgM	0.96 ng mL^{-1} for IgG 0.14 ng mL^{-1} for IgM	45 min	0.9928		217
	SARS-CoV-2 N-protein	56 fg mL^{-1}	1.5 min	0.99		218

of the SERS substrate has also affected the application of the SERS.

The SPR biosensor is highly affected by the RI of the sensing surface. The wavelength-dependent and angle-dependent biosensors are easily fabricated, while the architecture of the phase-dependent biosensors with higher sensitivity is more complicated. The SPR biosensor can be applied to detect SARS-CoV-2 in real-time. The SPR biosensor is highly affected by the temperature and the absorption of non-target analytes. In the measurement of the SRR, the reference liquid solvent has to be the same as the solvent that is applied for dissolving the analytes. This property limits the application of the SRR biosensors in the real sample.

FET biosensors rely on the changes in mobilities of channel materials caused by the bio-interaction, and the SPR biosensors are based on the "mass changing" of the sensing surface. FET is a continuous measurement that can be utilized in detecting SARS-CoV-2 in real-time. The channel material is the most important factor, which affects the performance and sensitivity. For 2D materials such as MoS_2 and WSe_2, it is hard to synthesize large areas of continuous 2D film. The application of the 2D flake is possible, but it needs a photograph to fabricate the source and drain electrodes. The large-scale chemical vapor deposition (CVD) graphene can be directly transferred on top of the prefabricated electrode, which reduces the fabrication difficulty. Moreover, the large-scale graphene with a uniform property makes the fabrication of the FET much easier, and the FET has more stable performance. Some other materials, such as carbon nanotubes and reduced graphene oxide, are spin-coated on the substrate and form a thin film. The inhomogeneous spin-coated film highly affects the performance of the FET and its reproducibility.

Fluorescence biosensors can detect SAR-CoV-2 at low concentrations with good sensitivity. For fluorescence biosensors, either bio-probes or analytes need to be modified with fluorophores, which can be excited and emit strong fluorescence. Normally, the modification requires several steps, and it requires an experienced biological background. This

disadvantage limits its application in detecting a large number of samples. Moreover, the unmodified fluorophores and the fluorescence background should be eliminated, which requires expensive equipment.

Electrochemical biosensors have properties of high selectivity and sensitivity, but they suffer from a lack of surface architectures, allowing the desired biochemical event. The electrode material, surface modification methods, or its dimensions heavily influence its detection ability. The proper architecture of the working electrodes can improve the specification and sensitivity of virus detection. The unexpected absorption of the organic or bio-compounds on the surface of working electrodes can result in the reduction of the working electrodes' mobilities and cause the failure of detection. As a surface sensing technique, it also is affected by the unexpected absorption of the non-target molecules. The detecting conditions, such as stirring, pH, and temperature, also affect the detecting reliabilities.

Until now, all of these nano-biosensors have been applied to detecting the real SARS-CoV-2 samples. Due to the applications of bio-probes, SARS-CoV-2 can be detected under good selectivity and sensitivity. In comparison with the pure analytes, the LOD is two or three orders of magnitudes larger. As surface sensing techniques, the bio events that occur on the surface are important and require some time. The "real-time" effects are always observed during the measurement in FET or SPR, but a cleaning step to remove the unexpectedly absorbed compounds is missing, which can confirm whether the signals are generated by the bio-interaction or not.

Until now, the re-utilization of the nano-biosensor has been rarely mentioned. For the SARS-CoV-2 nano-biosensor, the key scientific issue is to develop a reusable sensing surface such that the chemical or physically absorbed organic or biomolecules can be easily removed, and the sensitivity can be largely recovered. By conquering such a problem, the oropharyngeal swabs sampled from healthy people cannot affect the sensing surface, which enormously reduces the cost of detecting SARS-CoV-2.

12. Conclusion

COVID-19 has caused a huge disaster in the world. The pandemic of SARS-CoV-2 forced people to find a fast, efficient, easy, and cost-efficient detecting method. As a golden standard, the RT-PCR method meets the major bottleneck of lacking sufficient equipment, un-reusable reagents, and cost-consuming. Nowadays, there is a growing requirement for novel nano-biosensors with high selectivity and sensitivity. The principles of the SARS-CoV-2 nano-biosensor are an integration of physical/chemical principles with the bio-principle. The ACE2-S protein, ACE2-SARS-CoV-2 virus, S protein-antibody, antibody-IgG, antibody-IgM, and DNA probe-SARS-CoV-2 target oligonucleotide are the most used bio-pairs in the detection of SARS-CoV-2. By using the proper bio-probe, the nano-biosensors can selectively bind to the specific part of SARS-CoV-2, and the interactions between the probe and the target can be observed *via* optic or electrical signals. Moreover, some nano-biosensors possess the possibility of cyclic utilization, which reduces the cost of epidemiological investigation. Until now, the biosensor can reach a LOD of 1 copy per μL for the SARS-CoV-2 target oligonucleotide and 0.01 ag mL^{-1} for the SARS-CoV-2 spike antibody. The extremely low detection limits indicate a promising future for biosensors in detecting SARS-CoV-2.

In conclusion, this review highlights the current trends in SARS-CoV-2 nano-biosensors combined with optic and electric methods, and the improvement of these nano-biosensors. To face the present COVID-19 pandemic or the effective virus epidemic, it is necessary to have efficient virus sensing techniques at hand to help aid in the detection and prevention of viral spread.

Author contributions

Conceptualization, Yansheng Liu; writing—original draft preparation, Yansheng Liu and Zhenle Qin; review and editing, Jin Zhou, Xiaobo Jia, Hongli Li, Xiaohong Wang, Yating Chen, Zijun Sun, Xiong He, and Hongda Li; funding acquisition, Yansheng Liu and Guofu Wang; supervision, Haixin Chang; all authors have read and agreed to the published version of the manuscript.

Conflicts of interest

There are no conflicts to declare.

Acknowledgements

This work has been supported by the Guangxi Natural Science Foundation Project (No. 2021GXNSFBA196049), Guangxi Science and Technology Project (No. AD22035215), the National Key Research and Development Program of China (No. 2022YFE0134600 and No. 2021YFA0715404) and Guangxi Key Research and Development Program (No. 2021AB05083).

References

1 Y.-D. Li, W.-Y. Chi, J.-H. Su, L. Ferrall, C.-F. Hung and T. C. Wu, *J. Biomed. Sci.*, 2020, **27**, 104.
2 S. Lei, F. Jiang, W. Su, C. Chen, J. Chen, W. Mei, L.-Y. Zhan, Y. Jia, L. Zhang and D. Liu, *EClinicalMedicine*, 2020, **21**, 100331.
3 E. A. Meyerowitz, A. Richterman, R. T. Gandhi and P. E. Sax, *Ann. Intern. Med.*, 2020, **174**, 69–79.
4 W. Trypsteen, J. Van Cleemput, W. V. Snippenberg, S. Gerlo and L. Vandekerckhove, *PLoS Pathog.*, 2020, **16**, e1009037.
5 A. S. Lauring, M. W. Tenforde, J. D. Chappell, M. Gaglani, A. A. Ginde, T. McNeal, S. Ghamande, D. J. Douin, H. K. Talbot, J. D. Casey, N. M. Mohr, A. Zepeski, N. I. Shapiro, K. W. Gibbs, D. C. Files, D. N. Hager, A. Shehu, M. E. Prekker, H. L. Erickson, M. C. Exline, M. N. Gong, A. Mohamed, N. J. Johnson, V. Srinivasan, J. S. Steingrub, I. D. Peltan, S. M. Brown, E. T. Martin, A. S. Monto, A. Khan, C. L. Hough, L. W. Busse, C. C. Ten

Lohuis, A. Duggal, J. G. Wilson, A. J. Gordon, N. Qadir, S. Y. Chang, C. Mallow, C. Rivas, H. M. Babcock, J. H. Kwon, N. Halasa, C. G. Grijalva, T. W. Rice, W. B. Stubblefield, A. Baughman, K. N. Womack, J. P. Rhoads, C. J. Lindsell, K. W. Hart, Y. Zhu, K. Adams, S. J. Schrag, S. M. Olson, M. Kobayashi, J. R. Verani, M. M. Patel and W. H. Self, *medRxiv: the preprint server for health sciences*, 2022, DOI: 10.1101/2022.02.06.22270558.

6 T. P. Velavan and C. G. Meyer, *Trop. Med. Int. Health*, 2020, **25**, 278–280.

7 J. Cui, F. Li and Z.-L. Shi, *Nat. Rev. Microbiol.*, 2019, **17**, 181–192.

8 M. Yuce, E. Filiztekin and K. G. Ozkaya, *Biosens. Bioelectron.*, 2021, **172**, 112752.

9 N. Zhu, D. Zhang, W. Wang, X. Li, B. Yang, J. Song, X. Zhao, B. Huang, W. Shi, R. Lu, P. Niu, F. Zhan, X. Ma, D. Wang, W. Xu, G. Wu, G. F. Gao and W. Tan, *N. Engl. J. Med.*, 2020, **382**, 727–733.

10 R. A. Khailany, M. Safdar and M. Ozaslan, *Gene Rep.*, 2020, **19**, 100682.

11 A. C. Walls, Y.-J. Park, M. A. Tortorici, A. Wall, A. T. McGuire and D. Veesler, *Cell*, 2020, **181**, 281–292.e286.

12 S. Rosales-Mendoza, V. A. Márquez-Escobar, O. González-Ortega, R. Nieto-Gómez and J. I. Arévalo-Villalobos, *Vaccines*, 2020, **8**, 183.

13 P. Yang and X. Wang, *Cell. Mol. Immunol.*, 2020, **17**, 555–557.

14 E. Ong, M. U. Wong, A. Huffman and Y. He, *Front. Immunol.*, 2020, **11**, 1581.

15 A. B. Ryzhikov, G. S. Onkhonova, I. R. Imatdinov, E. V. Gavrilova, R. A. Maksyutov, E. A. Gordeeva, G. V. Pazynina, I. M. Ryzhov, N. V. Shilova and N. V. Bovin, *Biochemistry*, 2021, **86**, 243–247.

16 L. Wang and Y. Xiang, *Viruses*, 2020, **12**, 1289.

17 S. Xiaojie, L. Yu, Y. Lei, Y. Guang and Q. Min, *Stem Cell Res.*, 2020, **50**, 102125.

18 A. C. Walls, Y. J. Park, M. A. Tortorici, A. Wall, A. T. McGuire and D. Veesler, *Cell*, 2020, **181**, 281–292.e286.

19 Y. Huang, C. Yang, X.-f. Xu, W. Xu and S.-w. Liu, *Acta Pharmacol. Sin.*, 2020, **41**, 1141–1149.

20 M. Hoffmann, H. Kleine-Weber, S. Schroeder, N. Krüger, T. Herrler, S. Erichsen, T. S. Schiergens, G. Herrler, N.-H. Wu, A. Nitsche, M. A. Müller, C. Drosten and S. Pöhlmann, *Cell*, 2020, **181**, 271–280.e278.

21 S. Shahbaz, L. Xu, M. Osman, W. Sligl, J. Shields, M. Joyce, D. L. Tyrrell, O. Oyegbami and S. Elahi, *Stem Cell Rep.*, 2021, **16**, 1165–1181.

22 L. Shi, L. Wang, X. Ma, X. Fang, L. Xiang, Y. Yi, J. Li, Z. Luo and G. Li, *Anal. Chem.*, 2021, **93**, 16646–16654.

23 A. Tahamtan and A. Ardebili, *Expert Rev. Mol. Diagn.*, 2020, **20**, 453–454.

24 L. Lan, D. Xu, G. Ye, C. Xia, S. Wang, Y. Li and H. Xu, *Jama*, 2020, **323**, 1502–1503.

25 A. Avula, K. Nalleballe, N. Narula, S. Sapozhnikov, V. Dandu, S. Toom, A. Glaser and D. Elsayegh, *Brain, Behav., Immun.*, 2020, **87**, 115–119.

26 A. Singanayagam, M. Patel, A. Charlett, J. L. Bernal, V. Saliba, J. Ellis, S. Ladhani, M. Zambon and R. Gopal, *Eurosurveillance*, 2020, **25**, 2001483.

27 Y. Gong, K. Li, N. Copner, H. Liu, M. Zhao, B. Zhang, A. Pusch, D. L. Huffaker and S. S. Oh, *Nanophotonics*, 2021, **10**, 1285–1293.

28 L. Guo, L. Ren, S. Yang, M. Xiao, D. Chang, F. Yang, C. S. Dela Cruz, Y. Wang, C. Wu, Y. Xiao, L. Zhang, L. Han, S. Dang, Y. Xu, Q.-W. Yang, S.-Y. Xu, H.-D. Zhu, Y.-C. Xu, Q. Jin, L. Sharma, L. Wang and J. Wang, *Clin. Infect. Dis.*, 2020, **71**, 778–785.

29 R. A. Marsh and J. S. Orange, *Ann. Allergy, Asthma, Immunol.*, 2019, **123**, 444–453.

30 M. Hofreiter, V. Jaenicke, D. Serre, A. v. Haeseler and S. Pääbo, *Nucleic Acids Res.*, 2001, **29**, 4793–4799.

31 J. Li, D. Wu, Y. Yu, T. Li, K. Li, M. M. Xiao, Y. Li, Z. Y. Zhang and G. J. Zhang, *Biosens. Bioelectron.*, 2021, **183**, 113206.

32 R. Yan, Y. Zhang, Y. Li, L. Xia, Y. Guo and Q. Zhou, *Science*, 2020, **367**, 1444–1448.

33 F. Li, W. Li, M. Farzan and S. C. Harrison, *Science*, 2005, **309**, 1864–1868.

34 J. F.-W. Chan, K.-H. Kok, Z. Zhu, H. Chu, K. K.-W. To, S. Yuan and K.-Y. Yuen, *Emerging Microbes Infect.*, 2020, **9**, 221–236.

35 J. Brand, *Notes Rec. R. Soc. Lond.*, 1989, **43**, 1–23.

36 C. V. Raman, *Indian J. Phys.*, 1928, **2**, 387–398.

37 R. Krishnan and R. Shankar, *J. Raman Spectrosc.*, 1981, **10**, 1–8.

38 W. E. Huang, M. Li, R. M. Jarvis, R. Goodacre and S. A. Banwart, in *Advances in applied microbiology*, Elsevier, 2010, vol. 70, pp. 153–186.

39 E. C. Le Ru and P. G. Etchegoin, *Annu. Rev. Phys. Chem.*, 2012, **63**, 65–87.

40 K. A. Willets, *Chem. Soc. Rev.*, 2014, **43**, 3854–3864.

41 X. Ling, S. Huang, S. Deng, N. Mao, J. Kong, M. S. Dresselhaus and J. Zhang, *Acc. Chem. Res.*, 2015, **48**, 1862–1870.

42 Y. Liu and F. Luo, *Nano Res.*, 2019, **12**, 2788–2795.

43 S. Xu, S. Jiang, J. Wang, J. Wei, W. Yue and Y. Ma, *Sens. Actuators, B*, 2016, **222**, 1175–1183.

44 S. Nie and S. R. Emory, *Science*, 1997, **275**, 1102–1106.

45 F. Schedin, E. Lidorikis, A. Lombardo, V. G. Kravets, A. K. Geim, A. N. Grigorenko, K. S. Novoselov and A. C. Ferrari, *ACS Nano*, 2010, **4**, 5617–5626.

46 X. Huang, I. H. El-Sayed, W. Qian and M. A. El-Sayed, *J. Am. Chem. Soc.*, 2006, **128**, 2115–2120.

47 X. Ling, L. Xie, Y. Fang, H. Xu, H. Zhang, J. Kong, M. S. Dresselhaus, J. Zhang and Z. Liu, *Nano Lett.*, 2010, **10**, 553–561.

48 Y. Liu and F. Luo, *Nano Res.*, 2020, **13**, 138–144.

49 J. Langer, D. Jimenez de Aberasturi, J. Aizpurua, R. A. Alvarez-Puebla, B. Auguie, J. J. Baumberg, G. C. Bazan, S. E. J. Bell, A. Boisen, A. G. Brolo, J. Choo, D. Cialla-May, V. Deckert, L. Fabris, K. Faulds, F. J. Garcia de Abajo, R. Goodacre, D. Graham, A. J. Haes, C. L. Haynes, C. Huck, T. Itoh, M. Kall, J. Kneipp, N. A. Kotov, H. Kuang, E. C. Le Ru, H. K. Lee, J. F. Li,

X. Y. Ling, S. A. Maier, T. Mayerhofer, M. Moskovits, K. Murakoshi, J. M. Nam, S. Nie, Y. Ozaki, I. Pastoriza-Santos, J. Perez-Juste, J. Popp, A. Pucci, S. Reich, B. Ren, G. C. Schatz, T. Shegai, S. Schlucker, L. L. Tay, K. G. Thomas, Z. Q. Tian, R. P. Van Duyne, T. Vo-Dinh, Y. Wang, K. A. Willets, C. Xu, H. Xu, Y. Xu, Y. S. Yamamoto, B. Zhao and L. M. Liz-Marzan, *ACS Nano*, 2020, **14**, 28–117.

50 A. Otto, I. Mrozek, H. Grabhorn and W. Akemann, *J. Phys.: Condens. Matter*, 1992, **4**, 1143.

51 S. Yang, X. Dai, B. B. Stogin and T.-S. Wong, *Proc. Natl. Acad. Sci. U. S. A.*, 2016, **113**, 268–273.

52 W. Fan, Y. H. Lee, S. Pedireddy, Q. Zhang, T. Liu and X. Y. Ling, *Nanoscale*, 2014, **6**, 4843–4851.

53 Y. Zhao, D. Yang, X. Li, Y. Liu, X. Hu, D. Zhou and Y. Lu, *Nanoscale*, 2017, **9**, 1087–1096.

54 A. A. Balandin, S. Ghosh, W. Bao, I. Calizo, D. Teweldebrhan, F. Miao and C. N. Lau, *Nano Lett.*, 2008, **8**, 902–907.

55 P. Reokrungruang, I. Chatnuntawech, T. Dharakul and S. Bamrungsap, *Sens. Actuators, B*, 2019, **285**, 462–469.

56 Y. Liu, J. Deng, Z. Jin, T. Liu, J. Zhou, F. Luo and G. Wang, *Nano Res.*, 2022, **15**, 6062–6066.

57 Y. Wu, X. Wang, X. Wen, J. Zhu, X. Bai, T. Jia, H. Yang, L. Zhang and Y. Qi, *Phys. Lett. A*, 2020, 126544.

58 M. Vadai, D. K. Angell, F. Hayee, K. Sytwu and J. A. Dionne, *Nat. Commun.*, 2018, **9**, 1–8.

59 J.-A. Huang, M. Z. Mousavi, Y. Zhao, A. Hubarevich, F. Omeis, G. Giovannini, M. Schütte, D. Garoli and F. De Angelis, *Nat. Commun.*, 2019, **10**, 5321.

60 Y. Liu and F. Luo, *Nano Res.*, 2019, 1–8.

61 L. Zhang, H. Chang, A. Hirata, H. Wu, Q.-K. Xue and M. Chen, *ACS Nano*, 2013, **7**, 4595–4600.

62 J. U. Lee, W. H. Kim, H. S. Lee, K. H. Park and S. J. Sim, *Small*, 2019, **15**, 1804968.

63 S. G. Park, X. Xiao, J. Min, C. Mun, H. S. Jung, V. Giannini, R. Weissleder, S. A. Maier, H. Im and D. H. Kim, *Adv. Funct. Mater.*, 2019, **29**, 1904257.

64 M. Q. He, S. Chen, K. Yao, K. Wang, Y. L. Yu and J. H. Wang, *Small Methods*, 2019, **3**, 1900017.

65 Q. Lv, H. Min, D. B. Duan, W. Fang, G. M. Pan, A. G. Shen, Q. Q. Wang, G. Nie and J. M. Hu, *Adv. Healthcare Mater.*, 2019, **8**, 1801257.

66 P. Wang, M. Xia, O. Liang, K. Sun, A. F. Cipriano, T. Schroeder, H. Liu and Y. H. Xie, *Anal. Chem.*, 2015, **87**, 10255–10261.

67 L. Zhang, X. Li, Y. Wang, Q. Fu, Y. Tan, H. Wang, H. Chen and J. Zhou, *Sens. Actuators, B*, 2019, **279**, 503–508.

68 A. K. Nair, K. Bhavitha, S. Perumbilavil, P. Sankar, D. Rouxel, M. Kala, S. Thomas and N. Kalarikkal, *Carbon*, 2018, **132**, 380–393.

69 C. Carrillo-Carrión, R. Martínez, M. F. Navarro Poupard, B. Pelaz, E. Polo, A. Arenas-Vivo, A. Olgiati, P. Taboada, M. G. Soliman and Ú. Catalán, *Angew. Chem., Int. Ed.*, 2019, **58**, 7078–7082.

70 Q. Shi, D. E. Gómez, D. Dong, D. Sikdar, R. Fu, Y. Liu, Y. Zhao, D. M. Smilgies and W. Cheng, *Adv. Mater.*, 2019, **31**, 1900989.

71 X. Xia, J. Zeng, B. McDearmon, Y. Zheng, Q. Li and Y. Xia, *Angew. Chem., Int. Ed.*, 2011, **50**, 12542–12546.

72 Z. Li, Y. Gao, L. Zhang, Y. Fang and P. Wang, *Nanoscale*, 2018, **10**, 18720–18727.

73 J. R. Wang, C. Xia, L. Yang, Y. F. Li, C. M. Li and C. Z. Huang, *Anal. Chem.*, 2020, **92**, 4046–4052.

74 S. Ganesh, K. Venkatakrishnan and B. Tan, *Nat. Commun.*, 2020, **11**, 1135.

75 J.-A. Huang, M. Z. Mousavi, Y. Zhao, A. Hubarevich, F. Omeis, G. Giovannini, M. Schütte, D. Garoli and F. De Angelis, *Nat. Commun.*, 2019, **10**, 5321.

76 O. J. Achadu, N. Nwaji, D. Lee, J. Lee, E. M. Akinoglu, M. Giersig and E. Y. Park, *Nanoscale Adv.*, 2022, **4**, 871–883.

77 Y. Peng, C. Lin, L. Long, T. Masaki, M. Tang, L. Yang, J. Liu, Z. Huang, Z. Li, X. Luo, J. R. Lombardi and Y. Yang, *Nano-Micro Lett.*, 2021, **13**, 52.

78 D. Zhang, X. Zhang, R. Ma, S. Deng, X. Wang, X. Wang, X. Zhang, X. Huang, Y. Liu, G. Li, J. Qu, Y. Zhu and J. Li, *Water Res.*, 2021, **200**, 117243.

79 M. Zhang, X. Li, J. Pan, Y. Zhang, L. Zhang, C. Wang, X. Yan, X. Liu and G. Lu, *Biosens. Bioelectron.*, 2021, **190**, 113421.

80 L. Tong, H. Xu and M. Käll, *MRS Bull.*, 2014, **39**, 163–168.

81 C. Zhang, C. Li, J. Yu, S. Jiang, S. Xu, C. Yang, Y. J. Liu, X. Gao, A. Liu and B. Man, *Sens. Actuators, B*, 2018, **258**, 163–171.

82 L. Ma, Y.-L. Chen, D.-J. Yang, S.-J. Ding, L. Xiong, P.-L. Qin and X.-B. Chen, *J. Phys. Chem. C*, 2020, **124**, 25473–25479.

83 U. Dinish, G. Balasundaram, Y.-T. Chang and M. Olivo, *Sci. Rep.*, 2014, **4**, 1–7.

84 H. Liu, E. Dai, R. Xiao, Z. Zhou, M. Zhang, Z. Bai, Y. Shao, K. Qi, J. Tu, C. Wang and S. Wang, *Sens. Actuators, B*, 2021, **329**, 129196.

85 S. Chen, L. Meng, L. Wang, X. Huang, S. Ali, X. Chen, M. Yu, M. Yi, L. Li, X. Chen, L. Yuan, W. Shi and G. Huang, *Sens. Actuators, B*, 2021, **348**, 130706.

86 W. Liu, L. Liu, G. Kou, Y. Zheng, Y. Ding, W. Ni, Q. Wang, L. Tan, W. Wu and S. Tang, *J. Clin. Microbiol.*, 2020, **58**(6), DOI: 10.1128/jcm.00461-20.

87 R. Banerjee and A. Jaiswal, *Analyst*, 2018, **143**, 1970–1996.

88 L. Perico, S. Tomasoni, T. Peracchi, A. Perna, A. Pezzotta, G. Remuzzi and A. Benigni, *EBioMedicine*, 2020, **61**, 103069.

89 T. Nicol, C. Lefeuvre, O. Serri, A. Pivert, F. Joubaud, V. Dubée, A. Kouatchet, A. Ducancelle, F. Lunel-Fabiani and H. Le Guillou-Guillemette, *J. Clin. Virol.*, 2020, **129**, 104511.

90 S. Srivastav, A. Dankov, M. Adanalic, R. Grzeschik, V. Tran, S. Pagel-Wieder, F. Gessler, I. Spreitzer, T. Scholz, B. Schnierle, O. E. Anastasiou, U. Dittmer and S. Schlücker, *Anal. Chem.*, 2021, **93**, 12391–12399.

91 S. Yadav, M. A. Sadique, P. Ranjan, N. Kumar, A. Singhal, A. K. Srivastava and R. Khan, *ACS Appl. Bio Mater.*, 2021, **4**, 2974–2995.

92 S. Sloan-Dennison, E. O'Connor, J. W. Dear, D. Graham and K. Faulds, *Anal. Bioanal. Chem.*, 2022, **414**, 4541–4549.

93 R. Chen, C. Ren, M. Liu, X. Ge, M. Qu, X. Zhou, M. Liang, Y. Liu and F. Li, *ACS Nano*, 2021, **15**, 8996–9004.
94 K. Kim, L. Kashefi-Kheyrabadi, Y. Joung, K. Kim, H. Dang, S. G. Chavan, M.-H. Lee and J. Choo, *Sens. Actuators, B*, 2021, **329**, 129214.
95 J. Huang, J. Wen, M. Zhou, S. Ni, W. Le, G. Chen, L. Wei, Y. Zeng, D. Qi, M. Pan, J. Xu, Y. Wu, Z. Li, Y. Feng, Z. Zhao, Z. He, B. Li, S. Zhao, B. Zhang, P. Xue, S. He, K. Fang, Y. Zhao and K. Du, *Anal. Chem.*, 2021, **93**, 9174–9182.
96 F. Lussier, V. Thibault, B. Charron, G. Q. Wallace and J.-F. Masson, *TrAC, Trends Anal. Chem.*, 2020, **124**, 115796.
97 X. Lin, D. Lin, Y. Chen, J. Lin, S. Weng, J. Song and S. Feng, *Adv. Funct. Mater.*, 2021, **31**, 2103382.
98 H. Shin, S. Oh, S. Hong, M. Kang, D. Kang, Y.-g. Ji, B. H. Choi, K.-W. Kang, H. Jeong and Y. Park, *ACS Nano*, 2020, **14**, 5435–5444.
99 W. J. Thrift, S. Ronaghi, M. Samad, H. Wei, D. G. Nguyen, A. S. Cabuslay, C. E. Groome, P. J. Santiago, P. Baldi and A. I. Hochbaum, *ACS Nano*, 2020, **14**, 15336–15348.
100 Z. Fang, W. Wang, A. Lu, Y. Wu, Y. Liu, C. Yan and C. Han, Rapid classification of honey varieties by surface enhanced Raman scattering combining with deep learning, *2018 Cross Strait Quad-Regional Radio Science and Wireless Technology Conference (CSQRWC)*, IEEE, 2018, pp. 1–3.
101 S. Weng, W. Zhu, X. Zhang, H. Yuan, L. Zheng, J. Zhao, L. Huang and P. Han, *Artif. Intell. Agric.*, 2019, **3**, 1–10.
102 C. Carlomagno, D. Bertazioli, A. Gualerzi, S. Picciolini, P. I. Banfi, A. Lax, E. Messina, J. Navarro, L. Bianchi, A. Caronni, F. Marenco, S. Monteleone, C. Arienti and M. Bedoni, *Sci. Rep.*, 2021, **11**, 4943.
103 S. X. Leong, Y. X. Leong, E. X. Tan, H. Y. F. Sim, C. S. L. Koh, Y. H. Lee, C. Chong, L. S. Ng, J. R. T. Chen, D. W. C. Pang, L. B. T. Nguyen, S. K. Boong, X. Han, Y. C. Kao, Y. H. Chua, G. C. Phan-Quang, I. Y. Phang, H. K. Lee, M. Y. Abdad, N. S. Tan and X. Y. Ling, *ACS Nano*, 2022, **16**, 2629–2639.
104 N. Queralto, A. N. Berliner, B. Goldsmith, R. Martino, P. Rhodes and S. H. Lim, *J. Breath Res.*, 2014, **8**, 027112.
105 S. Grassin-Delyle, C. Roquencourt, P. Moine, G. Saffroy, S. Carn, N. Heming, J. Fleuriet, H. Salvator, E. Naline and L.-J. Couderc, *EBioMedicine*, 2021, **63**, 103154.
106 D. M. Ruszkiewicz, D. Sanders, R. O'Brien, F. Hempel, M. J. Reed, A. C. Riepe, K. Bailie, E. Brodrick, K. Darnley and R. Ellerkmann, *EClinicalMedicine*, 2020, **29**, 100609.
107 A. Amann, M. Corradi, P. Mazzone and A. Mutti, *Expert Rev. Mol. Diagn.*, 2011, **11**, 207–217.
108 K. Badjagbo, *Clin. Chem. Lab. Med.*, 2012, **50**, 1893–1902.
109 B. Liedberg, C. Nylander and I. Lundström, *Biosens. Bioelectron.*, 1995, **10**, i–ix.
110 I. Alves, C. Park and V. Hruby, *Curr. Protein Pept. Sci.*, 2005, **6**, 293–312.
111 P. Singh, *Sens. Actuators, B*, 2016, **229**, 110–130.
112 J. H. Qu, K. Leirs, W. Maes, M. Imbrechts, N. Callewaert, K. Lagrou, N. Geukens, J. Lammertyn and D. Spasic, *ACS Sens.*, 2022, **7**, 477–487.
113 J. N. Dash and R. Jha, *IEEE Photonics Technol. Lett.*, 2014, **26**, 595–598.
114 K. Matsubara, S. Kawata and S. Minami, *Appl. Opt.*, 1988, **27**, 1160–1163.
115 L. D. Maria and M. Martinelli, *Sens. Actuators, A*, 1992, **32**, 710–712.
116 X. Zhao, Z. Wang, F. Liang, Y. Cao and H. Xu, *Chinese J. Anal. Chem.*, 1998, **26**, 1320–1323.
117 Y.-F. Chang, W.-H. Wang, Y.-W. Hong, R.-Y. Yuan and K.-H. Chen, *Anal. Chem.*, 2018, **90**, 1861–1869.
118 Y.-F. Chang, W.-H. Wang, Y.-W. Hong, R.-Y. Yuan, K.-H. Chen, Y.-W. Huang, P.-L. Lu, Y.-H. Chen, Y.-M. A. Chen, L.-C. Su and S.-F. Wang, *Anal. Chem.*, 2018, **90**, 1861–1869.
119 K. E. B. Thornton, D. Uttamchandani and B. Culshaw, *Electron. Lett.*, 1986, **22**, 1232–1234.
120 J. Homola, J. Dostálek, S. Chen, A. Rasooly, S. Jiang and S. S. Yee, *Int. J. Food Microbiol.*, 2002, **75**, 61–69.
121 X. Liu, *Anal. Biochem.*, 2003, **314**, 301–309.
122 Y. Tian, W. Zhang, D. Song, Y. Cao, X. Liu, H. Zhang and X. U. Han, *Chem. Res. Chin. Univ.*, 2004, **25**, 441–444.
123 H. Yan, G. Lai-xu, L. Song-quan, S. Wen-ling and Y. Hong-an, Research on Surface Plasmon Resonance Sensor Based on Wavelength Modulation by Using Theoretical Simulation Resonance Sensor Based on Wavelength Modulation by Using Theoretical Simulation, *2011 Third International Conference on Measuring Technology and Mechatronics Automation*, Shanghai, China, 2011, pp. 83–86, DOI: 10.1109/ICMTMA.2011.592.
124 S. P. Ng, C. M. L. Wu, S. Y. Wu and H. P. Ho, *Opt. Express*, 2011, **19**, 4521–4527.
125 P. Hlubina, J. Luňáček, D. Ciprian and R. Chlebus, *Opt. Commun.*, 2008, **281**, 2349–2354.
126 Q. Kemao, *Opt. Lasers Eng.*, 2007, **45**, 304–317.
127 G. Qiu, Z. Gai, Y. Tao, J. Schmitt, G. A. Kullak-Ublick and J. Wang, *ACS Nano*, 2020, **14**, 5268–5277.
128 W. K. Yeung, S. C. Lo, S. H. Wang, P. K. Wei and J. Y. Cheng, *Analyst*, 2021, **146**, 5584–5591.
129 I. Plikusiene, V. Maciulis, A. Ramanaviciene, Z. Balevicius, E. Buzavaite-Verteliene, E. Ciplys, R. Slibinskas, M. Simanavicius, A. Zvirbliene and A. Ramanavicius, *J. Colloid Interface Sci.*, 2021, **594**, 195–203.
130 C. M. Das, Y. Guo, G. Yang, L. Kang, G. Xu, H. P. Ho and K. T. Yong, *Adv. Theory Simul.*, 2020, **3**, 2000185.
131 M. Couture, Y. Liang, H.-P. P. Richard, R. Faid, W. Peng and J.-F. Masson, *Nanoscale*, 2013, **5**, 12399–12408.
132 J. Song, P. Huang, H. Duan and X. Chen, *J. Acc. Chem. Res.*, 2015, **48**, 2506–2515.
133 A. Samavati, Z. Samavati, M. Velashjerdi, A. Fauzi Ismail, M. H. D. Othman, B. G. Eisaabadi, M. Sohaimi Abdullah, M. Bolurian and M. Bolurian, *Chem. Eng. J.*, 2021, **420**, 127655.
134 E. Cesewski and B. N. Johnson, *Biosens. Bioelectron.*, 2020, **159**, 112214.
135 Y. Liang, M. Xiao, D. Wu, Y. Lin, L. Liu, J. He, G. Zhang, L.-M. Peng and Z. Zhang, *ACS Nano*, 2020, **14**, 8866–8874.
136 L. Syedmoradi, A. Ahmadi, M. L. Norton and K. Omidfar, *Microchim. Acta*, 2019, **186**, 739.
137 Y. Song, Y. Luo, C. Zhu, H. Li, D. Du and Y. Lin, *Biosens. Bioelectron.*, 2016, **76**, 195–212.

138 S. Mao, J. Chang, H. Pu, G. Lu, Q. He, H. Zhang and J. Chen, *Chem. Soc. Rev.*, 2017, **46**, 6872–6904.
139 G. Seo, G. Lee, M. J. Kim, S. H. Baek, M. Choi, K. B. Ku, C. S. Lee, S. Jun, D. Park, H. G. Kim, S. J. Kim, J. O. Lee, B. T. Kim, E. C. Park and S. I. Kim, *ACS Nano*, 2020, **14**, 5135–5142.
140 P. Blake, E. Hill, A. Castro Neto, K. Novoselov, D. Jiang, R. Yang, T. Booth and A. Geim, *Appl. Phys. Lett.*, 2007, **91**, 063124.
141 C. N. R. Rao, A. K. Sood, K. S. Subrahmanyam and A. Govindaraj, *Angew. Chem., Int. Ed.*, 2009, **48**, 7752–7777.
142 K. S. Novoselov, A. K. Geim, S. V. Morozov, D. Jiang, Y. Zhang, S. V. Dubonos, I. V. Grigorieva and A. A. Firsov, *Science*, 2004, **306**, 666–669.
143 K. S. Novoselov, A. K. Geim, S. V. Morozov, D. Jiang, M. I. Katsnelson, I. V. Grigorieva, S. V. Dubonos and A. A. Firsov, *Nature*, 2005, **438**, 197–200.
144 Y. Zhang, Y.-W. Tan, H. L. Stormer and P. Kim, *Nature*, 2005, **438**, 201–204.
145 K. S. Novoselov, Z. Jiang, Y. Zhang, S. Morozov, H. L. Stormer, U. Zeitler, J. Maan, G. Boebinger, P. Kim and A. K. Geim, *Science*, 2007, **315**, 1379.
146 M. Y. Han, B. Özyilmaz, Y. Zhang and P. Kim, *Phys. Rev. Lett.*, 2007, **98**, 206805.
147 M. C. Lemme, T. J. Echtermeyer, M. Baus and H. Kurz, *IEEE Electron Device Lett.*, 2007, **28**, 282–284.
148 Y. Zhang, J. P. Small, W. V. Pontius and P. Kim, *Appl. Phys. Lett.*, 2005, **86**, 073104.
149 A. C. Ferrari, J. Meyer, V. Scardaci, C. Casiraghi, M. Lazzeri, F. Mauri, S. Piscanec, D. Jiang, K. Novoselov and S. Roth, *Phys. Rev. Lett.*, 2006, **97**, 187401.
150 J. S. Bunch, A. M. Van Der Zande, S. S. Verbridge, I. W. Frank, D. M. Tanenbaum, J. M. Parpia, H. G. Craighead and P. L. McEuen, *Science*, 2007, **315**, 490–493.
151 P. Blake, P. D. Brimicombe, R. R. Nair, T. J. Booth, D. Jiang, F. Schedin, L. A. Ponomarenko, S. V. Morozov, H. F. Gleeson and E. W. Hill, *Nano Lett.*, 2008, **8**, 1704–1708.
152 X. Huang, X. Qi, F. Boey and H. Zhang, *Chem. Soc. Rev.*, 2012, **41**, 666–686.
153 X. Du, I. Skachko, A. Barker and E. Y. Andrei, *Nat. Nanotechnol.*, 2008, **3**, 491.
154 X. Jin, H. Zhang, Y. T. Li, M. M. Xiao, Z. L. Zhang, D. W. Pang, G. Wong, Z. Y. Zhang and G. J. Zhang, *Microchim. Acta*, 2019, **186**, 223.
155 L. Wu, J. Guo, Q. Wang, S. Lu, X. Dai, Y. Xiang and D. Fan, *Sens. Actuators, B*, 2017, **249**, 542–548.
156 S. Islam, S. Shukla, V. K. Bajpai, Y.-K. Han, Y. S. Huh, A. Kumar, A. Ghosh and S. Gandhi, *Biosens. Bioelectron.*, 2019, **126**, 792–799.
157 D. Wu, Y. Yu, D. Jin, M.-M. Xiao, Z.-Y. Zhang and G.-J. Zhang, *Anal. Chem.*, 2020, **92**, 4006–4015.
158 Y. Yu, Y. T. Li, D. Jin, F. Yang, D. Wu, M. M. Xiao, H. Zhang, Z. Y. Zhang and G. J. Zhang, *Anal. Chem.*, 2019, **91**, 10679–10686.
159 M. T. Hwang, I. Park, M. Heiranian, A. Taqieddin, S. You, V. Faramarzi, A. A. Pak, A. M. van der Zande, N. R. Aluru and R. Bashir, *Adv. Mater. Technol.*, 2021, **6**, 2100712.
160 E. Piccinini, G. E. Fenoy, A. L. Cantillo, J. A. Allegretto, J. Scotto, J. M. Piccinini, W. A. Marmisollé and O. Azzaroni, *Adv. Mater. Interfaces*, 2022, **9**, 2102526.
161 M. A. Zamzami, G. Rabbani, A. Ahmad, A. A. Basalah, W. H. Al-Sabban, S. Nate Ahn and H. Choudhry, *Bioelectrochemistry*, 2022, **143**, 107982.
162 W. Shao, M. R. Shurin, S. E. Wheeler, X. He and A. Star, *ACS Appl. Mater. Interfaces*, 2021, **13**, 10321–10327.
163 J. Kong, R. Franklin Nathan, C. Zhou, G. Chapline Michael, S. Peng, K. Cho and H. Dai, *Science*, 2000, **287**, 622–625.
164 M. S. Dresselhaus, G. Dresselhaus and P. C. Eklund, *Science of fullerenes and carbon nanotubes: their properties and applications*, Elsevier, 1996.
165 K. Balasubramanian and K. Kern, *Adv. Mater.*, 2014, **26**, 1154–1175.
166 M. Thanihaichelvan, S. N. Surendran, T. Kumanan, U. Sutharsini, P. Ravirajan, R. Valluvan and T. Tharsika, *Mater. Today: Proc.*, 2022, **49**, 2546–2549.
167 J. Wei, Z. Zhao, F. Luo, K. Lan, R. Chen and G. Qin, *2D Mater.*, 2021, **9**, 015030.
168 P. Fathi-Hafshejani, N. Azam, L. Wang, M. A. Kuroda, M. C. Hamilton, S. Hasim and M. Mahjouri-Samani, *ACS Nano*, 2021, **15**, 11461–11469.
169 N. Masurkar, N. K. Thangavel, S. Yurgelevic, S. Varma, G. W. Auner and L. M. Reddy Arava, *Biosens. Bioelectron.*, 2021, **172**, 112724.
170 K. Kalantar-zadeh and J. Z. Ou, *ACS Sens.*, 2016, **1**, 5–16.
171 K. S. Novoselov, A. K. Geim, S. V. Morozov, D. Jiang, M. I. Katsnelson, I. Grigorieva and S. Dubonos, Firsov and AA, *Nature*, 2005, **438**, 197–200.
172 A. K. Geim and K. S. Novoselov, in *Nanoscience and Technology: A Collection of Reviews from Nature Journals*, World Scientific, 2010, pp. 11–19.
173 X. Ling, W. Fang, Y. H. Lee, P. T. Araujo, X. Zhang, J. F. Rodriguez-Nieva, Y. Lin, J. Zhang, J. Kong and M. S. Dresselhaus, *Nano Lett.*, 2014, **14**, 3033–3040.
174 T. Shimada, K. Hamaguchi, A. Koma and F. Ohuchi, *Appl. Phys. Lett.*, 1998, **72**, 1869–1871.
175 H. Jiang, *J. Phys. Chem. C*, 2012, **116**, 7664–7671.
176 W. Liu, J. Kang, D. Sarkar, Y. Khatami, D. Jena and K. Banerjee, *Nano Lett.*, 2013, **13**, 1983–1990.
177 B. Doppagne, T. Neuman, R. Soria-Martinez, L. E. P. López, H. Bulou, M. Romeo, S. Berciaud, F. Scheurer, J. Aizpurua and G. Schull, *Nat. Nanotechnol.*, 2020, **15**, 207–211.
178 R. Weissleder and V. Ntziachristos, *Nat. Med.*, 2003, **9**, 123–128.
179 X. Chen, K. Xu, J. Li, M. Yang, X. Li, Q. Chen, C. Lu and H. Yang, *Biosens. Bioelectron.*, 2020, **155**, 112104.
180 E. Benito-Pena, M. G. Valdes, B. Glahn-Martinez and M. C. Moreno-Bondi, *Anal. Chim. Acta*, 2016, **943**, 17–40.
181 M. Bauch, K. Toma, M. Toma, Q. Zhang and J. Dostalek, *Plasmonics*, 2014, **9**, 781–799.
182 M. Wang, Y. Lin, J. Lu, Z. Sun, Y. Deng, L. Wang, Y. Yi, J. Li, J. Yang and G. Li, *Chem. Eng. J.*, 2022, **429**, 132332.

183 S. K. Krishnan, E. Singh, P. Singh, M. Meyyappan and H. S. Nalwa, *RSC Adv.*, 2019, **9**, 8778–8881.
184 N. C. Cady, N. Tokranova, A. Minor, N. Nikvand, K. Strle, W. T. Lee, W. Page, E. Guignon, A. Pilar and G. N. Gibson, *Biosens. Bioelectron.*, 2021, **171**, 112679.
185 B. Kang, Y. Lee, J. Lim, D. Yong, Y. Ki Choi, S. Woo Yoon, S. Seo, S. Jang, S. Uk Son, T. Kang, J. Jung, K.-S. Lee, M. H. Kim and E.-K. Lim, *Chem. Eng. J.*, 2022, **442**, 136143.
186 G. R. Bardajee, M. Zamani, M. Sharifi, H. Rezanejad and M. Motallebi, *J. Fluoresc.*, 2022, **32**, 1959–1967.
187 G. R. Bardajee, M. Zamani, H. Mahmoodian, H. Elmizadeh, H. Yari, L. Jouyandeh, R. Shirkavand and M. Sharifi, *Spectrochim. Acta, Part Ac*, 2022, **269**, 120702.
188 N. H. T. Tran, K. T. L. Trinh, J. H. Lee, W. J. Yoon and H. Ju, *Small*, 2018, **14**, 1801385.
189 Z. Zhu, P. Yuan, S. Li, M. Garai, M. Hong and Q.-H. Xu, *ACS Appl. Bio Mater.*, 2018, **1**, 118–124.
190 K. E. Sapsford, L. Berti and I. L. Medintz, *Angew. Chem., Int. Ed. Engl.*, 2006, **45**, 4562–4589.
191 J. Han, H. Y. Zou, M. X. Gao and C. Z. Huang, *Talanta*, 2016, **148**, 279–284.
192 F. Tian, J. Lyu, J. Shi and M. Yang, *Biosens. Bioelectron.*, 2017, **89**, 123–135.
193 E. Ploetz, E. Lerner, F. Husada, M. Roelfs, S. Chung, J. Hohlbein, S. Weiss and T. Cordes, *Sci. Rep.*, 2016, **6**, 33257.
194 R. Roy, S. Hohng and T. Ha, *Nat. Methods*, 2008, **5**, 507.
195 E. A. Jares-Erijman and T. M. Jovin, *Nat. Biotechnol.*, 2003, **21**, 1387.
196 K. Girigoswami and N. Akhtar, *Int. J. Nano Dimens.*, 2019, **10**, 1–17.
197 H. Ueda and J. Dong, *Biochim. Biophys. Acta, Proteins Proteomics*, 2014, **1844**, 1951–1959.
198 X. Li, Z.-Q. Dong, P. Yu, L.-P. Wang, X.-D. Niu, H. Yamaguchi and D.-C. Li, *Phys. Fluids*, 2021, **33**, 042004.
199 G. Balkourani, A. Brouzgou, M. Archonti, N. Papandrianos, S. Song and P. Tsiakaras, *J. Electroanal. Chem.*, 2021, **893**, 115289.
200 F. Zhao, Y. Bai, L. Cao, G. Han, C. Fang, S. Wei and Z. Chen, *J. Electroanal. Chem.*, 2020, **867**, 114184.
201 H. Ilkhani and S. Farhad, *Anal. Biochem.*, 2018, **557**, 151–155.
202 Q. Gong, H. Han, H. Yang, M. Zhang, X. Sun, Y. Liang, Z. Liu, W. Zhang and J. Qiao, *J. Materiomics*, 2019, **5**, 313–319.
203 G. Martins, J. L. Gogola, F. R. Caetano, C. Kalinke, T. R. Jorge, C. N. D. Santos, M. F. Bergamini and L. H. Marcolino-Junior, *Talanta*, 2019, **204**, 163–171.
204 J. Huang, J. Meng, S. Chen, S. Zhang, T. Liu, C. Li and F. Wang, *Biosens. Bioelectron.*, 2020, **164**, 112310.
205 J. Wang and J. W. Schultze, *Angew. Chem., Int. Ed. Engl.*, 1996, **35**, 1998.
206 L. Liv, *Microchem. J.*, 2021, **168**, 106445.
207 H. Zhao, F. Liu, W. Xie, T.-C. Zhou, J. OuYang, L. Jin, H. Li, C.-Y. Zhao, L. Zhang, J. Wei, Y.-P. Zhang and C.-P. Li, *Sens. Actuators, B*, 2021, **327**, 128899.
208 L. Farzin, S. Sadjadi, A. Sheini and E. Mohagheghpour, *Mikrochim. Acta*, 2021, **188**, 121.
209 N. J. Ronkainen, H. B. Halsall and W. R. Heineman, *Chem. Soc. Rev.*, 2010, **39**, 1747–1763.
210 V. K. Gupta, R. Jain, K. Radhapyari, N. Jadon and S. Agarwal, *Anal. Biochem.*, 2011, **408**, 179.
211 F. Patolsky, Y. Weizmann and I. Willner, *J. Am. Chem. Soc.*, 2002, **124**, 770–772.
212 A. J. Blasco, M. C. González and A. Escarpa, *Anal. Chim. Acta*, 2004, **511**, 71–81.
213 B. J. Venton and D. J. DiScenza, in *Electrochemistry for Bioanalysis*, ed. B. Patel, Elsevier, 2020, pp. 27–50, DOI: 10.1016/B978-0-12-821203-5.00004-X.
214 P. Westbroek, in *Analytical Electrochemistry in Textiles*, ed. P. Westbroek, G. Priniotakis and P. Kiekens, Woodhead Publishing, 2005, pp. 37–69, DOI: 10.1533/9781845690878.1.37.
215 J. C. Abrego-Martinez, M. Jafari, S. Chergui, C. Pavel, D. Che and M. Siaj, *Biosens. Bioelectron.*, 2022, **195**, 113595.
216 J. Zeng, P. A. Duarte, Y. Ma, O. Savchenko, L. Shoute, Y. Khaniani, S. Babiuk, R. Zhuo, G. N. Abdelrasoul, C. Charlton, J. N. Kanji, L. Babiuk, C. Edward and J. Chen, *Biosens. Bioelectron.*, 2022, **213**, 114476.
217 A. Yakoh, U. Pimpitak, S. Rengpipat, N. Hirankarn, O. Chailapakul and S. Chaiyo, *Biosens. Bioelectron.*, 2021, **176**, 112912.
218 R. Salahandish, P. Jalali, H. O. Tabrizi, J. E. Hyun, F. Haghayegh, M. Khalghollah, A. Zare, B. M. Berenger, Y. D. Niu, E. Ghafar-Zadeh and A. Sanati-Nezhad, *Biosens. Bioelectron.*, 2022, **213**, 114459.
219 S. D. Bukkitgar, N. P. Shetti, R. M. Kulkarni, K. R. Reddy, S. S. Shukla, V. S. Saji and T. M. Aminabhavi, *J. Electrochem. Soc.*, 2019, **166**, B3072–B3078.
220 N. P. Shetti, S. J. Malode, D. S. Nayak, G. B. Bagihalli, S. S. Kalanur, R. S. Malladi, C. V. Reddy, T. M. Aminabhavi and K. R. Reddy, *Appl. Surf. Sci.*, 2019, **496**, 143656.
221 S. D. Bukkitgar, N. P. Shetti and T. M. Aminabhavi, *Chem. Eng. J.*, 2021, **420**.
222 Y. Peng, Y. Pan, Z. Sun, J. Li, Y. Yi, J. Yang and G. Li, *Biosens. Bioelectron.*, 2021, **186**, 113309.
223 Y. Deng, T. Zhou, Y. Peng, M. Wang, L. Xiang, Y. Zhang, J. Li, J. Yang and G. Li, *Anal. Chem.*, 2023, **95**, 3358–3362.
224 Y. Deng, Y. Peng, L. Wang, M. Wang, T. Zhou, L. Xiang, J. Li, J. Yang and G. Li, *Anal. Chim. Acta*, 2022, **1208**, 339846.
225 Q. Liang, Y. Huang, M. Wang, D. Kuang, J. Yang, Y. Yi, H. Shi, J. Li, J. Yang and G. Li, *Chem. Eng. J.*, 2023, **452**, 139646.
226 L. Yin, S. Man, S. Ye, G. Liu and L. Ma, *Biosens. Bioelectron.*, 2021, **193**, 113541.
227 J. S. Park, K. Hsieh, L. Chen, A. Kaushik, A. Y. Trick and T. H. Wang, *Adv. Sci.*, 2021, **8**, 2003564.
228 A. Ramachandran, D. A. Huyke, E. Sharma, M. K. Sahoo, C. Huang, N. Banaei, B. A. Pinsky and J. G. Santiago, *Proc. Natl. Acad. Sci. U. S. A.*, 2020, **117**, 29518–29525.
229 A. Santiago-Frangos, A. Nemudryi, A. Nemudraia, T. Wiegand, J. E. Nichols, P. Krishna, A. M. Scherffius,

T. R. Zahl, R. A. Wilkinson and B. Wiedenheft, *Methods*, 2022, **205**, 1–10.

230 L. Wang, R. He, B. Lv, X. Yu, Y. Liu, J. Yang, W. Li, Y. Wang, H. Zhang, G. Yan, W. Mao, L. Liu, F. Wang and L. Ma, *Talanta*, 2021, **227**, 122154.

231 X. Ye, H. Zhou, X. Guo, D. Liu, Z. Li, J. Sun, J. Huang, T. Liu, P. Zhao, H. Xu, K. Li, H. Wang, J. Wang, L. Wang, W. Zhao, Q. Liu, S. Xu and Y. Feng, *Biosens. Bioelectron.*, 2022, **207**, 114169.

232 Y. Li, J. Qiao, X. Han, Z. Zhao, J. Kou, W. Zhang, S. Man and L. Ma, *Viruses*, 2022, **15**, 120.

233 F. E. Chen, P. W. Lee, A. Y. Trick, J. S. Park, L. Chen, K. Shah, H. Mostafa, K. C. Carroll, K. Hsieh and T. H. Wang, *Biosens. Bioelectron.*, 2021, **190**, 113390.

234 A. Santiago-Frangos, L. N. Hall, A. Nemudraia, A. Nemudryi, P. Krishna, T. Wiegand, R. A. Wilkinson, D. T. Snyder, J. F. Hedges, C. Cicha, H. H. Lee, A. Graham, M. A. Jutila, M. P. Taylor and B. Wiedenheft, *Cell Rep. Med.*, 2021, **2**, 100319.

235 L. Ma, W. Zhang, L. Yin, Y. Li, J. Zhuang, L. Shen and S. Man, *J. Hazard. Mater.*, 2023, **452**, 131195.

236 F. Wang, J. Yang, R. He, X. Yu, S. Chen, Y. Liu, L. Wang, A. Li, L. Liu, C. Zhai and L. Ma, *Biosens. Bioelectron.*, 2021, **177**, 112932.

237 J. Li, L. Tang, T. Li, K. Li, Y. Zhang, W. Ni, M. M. Xiao, Y. Zhao, Z. Y. Zhang and G. J. Zhang, *ACS Sens.*, 2022, **7**, 2680–2690.

238 Q. H. Nguyen and M. I. Kim, *Trends Anal. Chem.*, 2020, **132**, 116038.

239 L. Tessaro, A. Aquino, P. Panzenhagen, N. Joshi and C. A. Conte-Junior, *J. Pharm. Biomed. Anal.*, 2023, **222**, 115087.

240 Z. Ali, R. Aman, A. Mahas, G. S. Rao, M. Tehseen, T. Marsic, R. Salunke, A. K. Subudhi, S. M. Hala, S. M. Hamdan, A. Pain, F. S. Alofi, A. Alsomali, A. M. Hashem, A. Khogeer, N. A. M. Almontashiri, M. Abedalthagafi, N. Hassan and M. M. Mahfouz, *Virus Res.*, 2020, **288**, 198129.

241 E. Karakus, E. Erdemir, N. Demirbilek and L. Liv, *Anal. Chim. Acta*, 2021, **1182**, 338939.

242 M. Alafeef, P. Moitra, K. Dighe and D. Pan, *Nat. Protoc.*, 2021, **16**, 3141–3162.

243 W. Ren and J. Irudayaraj, *Biosensors*, 2021, **11**, 488.

244 K. Behrouzi and L. Lin, *Biosens. Bioelectron.*, 2022, **195**, 113669.

245 A. Vaquer, A. Alba-Patino, C. Adrover-Jaume, S. M. Russell, M. Aranda, M. Borges, J. Mena, A. Del Castillo, A. Socias, L. Martin, M. M. Arellano, M. Agudo, M. Gonzalez-Freire, M. Besalduch, A. Clemente, E. Baron and R. de la Rica, *Sens. Actuators, B*, 2021, **345**, 130347.

246 A. L. Ferreira, L. F. de Lima, M. T. Torres, W. R. de Araujo and C. de la Fuente-Nunez, *ACS Nano*, 2021, **15**, 17453–17462.

247 S. Cavalera, B. Colitti, S. Rosati, G. Ferrara, L. Bertolotti, C. Nogarol, C. Guiotto, C. Cagnazzo, M. Denina, F. Fagioli, F. Di Nardo, M. Chiarello, C. Baggiani and L. Anfossi, *Talanta*, 2021, **223**, 121737.

248 A. Bhattacharjee, R. M. Sabino, J. Gangwish, V. K. Manivasagam, S. James, K. C. Popat, M. Reynolds and Y. V. Li, *In Vitro Models*, 2022, **1**, 241–247.

249 L. Wu, A. Garrido-Maestu, J. R. L. Guerreiro, S. Carvalho, S. Abalde-Cela, M. Prado and L. Diéguez, *Nanoscale*, 2019, **11**, 7781–7789.

250 J.-A. Huang, M. Z. Mousavi, Y. Zhao, A. Hubarevich, F. Omeis, G. Giovannini, M. Schütte, D. Garoli and F. De Angelis, *Nat. Commun.*, 2019, **10**, 1–10.

251 Z. He, Z. Han, M. Kizer, R. J. Linhardt, X. Wang, A. M. Sinyukov, J. Wang, V. Deckert, A. V. Sokolov, J. Hu and M. O. Scully, *J. Am. Chem. Soc.*, 2019, **141**, 753–757.

252 T. Zhang, R. Deng, Y. Wang, C. Wu, K. Zhang, C. Wang, N. Gong, R. Ledesma-Amaro, X. Teng and C. Yang, *Nat. Biomed. Eng.*, 2022, 1–11.

253 K. M. Cheung, J. M. Abendroth, N. Nakatsuka, B. Zhu, Y. Yang, A. M. Andrews and P. S. Weiss, *Nano Lett.*, 2020, **20**, 5982–5990.

254 S. Tripathy, R. Gangwar, P. Supraja, A. N. Rao, S. R. K. Vanjari and S. G. Singh, *Electroanalysis*, 2018, **30**, 2110–2120.

255 R. Zhang, X. Zhang, H. Wang, Y. Zhang, S. Jiang, C. Hu, Y. Zhang, Y. Luo and Z. Dong, *Angew. Chem., Int. Ed.*, 2017, **56**, 5561–5564.

256 F. Pashaee, M. Tabatabaei, F. A. Caetano, S. S. Ferguson and F. Lagugne-Labarthet, *Analyst*, 2016, **141**, 3251–3258.

257 K. H. Ooi, M. M. Liu, J. W. D. Tay, S. Y. Teo, P. Kaewsapsak, S. Jin, C. K. Lee, J. Hou, S. Maurer-Stroh and W. Lin, *Nat. Commun.*, 2021, **12**, 1–23.

258 T. A. Yano, T. Kajisa, M. Ono, Y. Miyasaka, Y. Hasegawa, A. Saito, K. Otsuka, A. Sakane, T. Sasaki, K. Yasutomo, R. Hamajima, Y. Kanai, T. Kobayashi, Y. Matsuura, M. Itonaga and T. Yasui, *Sci. Rep.*, 2022, **12**, 1060.

259 D. Song, J. Liu, W. Xu, X. Han, H. Wang, Y. Cheng, Y. Zhuo and F. Long, *Talanta*, 2021, **235**, 122800.